The Thesis Committee for Colin Stephen Doyle
Certifies that this is the approved version of the following thesis:

Leveraging Geospatial Technologies for Flood Management and Disaster Assessment in the Lower Mekong River Basin

APPROVED BY
SUPERVISING COMMITTEE:

Supervisor:

Timothy Beach

Sheryl Luzzadder-Beach

John Bolten

Leveraging Geospatial Technologies for Flood Management and Disaster Assessment in the Lower Mekong River Basin

by

Colin Doyle

Thesis

Presented to the Faculty of the Graduate School of

The University of Texas at Austin

in Partial Fulfillment

of the Requirements

for the Degree of

Master of Arts

The University of Texas at Austin

August, 2017

Acknowledgements

I would like to thank the NASA DEVELOP National Program and NASA Goddard Space Flight Center for providing the resources and opportunity to begin my research on using geospatial technologies to study flooding in Southeast Asia. Specifically, I would like to thank John Bolten (NASA GSFC) and Joseph Spruce (Computer Science Corp, NASA SSC) who provided feedback and guidance in developing flood-mapping methods. I would also like to thank my graduate advisors Timothy Beach and Sheryl Luzzadder-Beach (University of Texas at Austin) and the Department of Geography and the Environment for providing the resources and support to complete the entirety of this Master's Thesis.

Abstract

Leveraging Geospatial Technologies for Flood Management and Disaster Assessment in the Lower Mekong River Basin

Colin Stephen Doyle, MA

The University of Texas at Austin, 2017

Supervisor: Timothy Beach

The sixty million inhabitants of the Lower Mekong River Basin (LMB) in Southeast Asia rely on the natural resources provided by the Mekong River and its annual flooding. Extreme events, however, can cause widespread agricultural, structural, and humanitarian loss across the basin. Population increases, land use change, hydropower development, and climate change threaten to increase flood risk and potential damage over the next century. Geospatial technologies such as satellite remote sensing and Geographic Information Systems (GIS) provide powerful tools for assessing historic risk and monitoring real-time events. In this thesis, I first assess trends in flood magnitude and timing over the last 90 years using stream gauge data to understand changes in the annual flooding of the river and associated risk. Next, I develop methods for using satellite data to map flood extent and relative degree, as well as assess risk to agriculture from both floods and droughts based on historic conditions. Lastly, I demonstrate how the satellite-derived flood maps can be integrated with socio-economic data in automated GIS tools to provide timely and reliable estimates of socio-economic damage during disasters.

Table of Contents

List of Tables viii

List of Figures ix

Chapter 1: Introduction 1

Study Area 2

Chapter 2: Recent Changes in Annual Flooding 7

Introduction 7

Methodology 8

Results and Discussion 11

Trends in Peak Discharge 11

Flood Recurrence 13

Timing and Length of Flood Season 16

Conclusions 19

Chapter 3: Monitoring Mekong Flooding from Space 21

Introduction 21

Methodology 24

Flood Detection 24

Validation 29

Results and Discussion 32

Conclusions 41

Chapter 4: Detecting Rice Agriculture at Risk to Extreme Flood and Drought Conditions 45

Introduction 45

Detecting flood and drought damage 47

Methodology 48

Results and Discussion 50

Conclusions 55

Chapter 5: GIS and Remote Sensing for Rapid Socio-economic Impact Assessment 58
Introduction 58
Current Practices 58
Methodology 60
Deriving Flood Map 60
Estimating Socio-economic Impacts 61
Results and Discussion 66
Conclusions 69
Chapter 6: Concluding Remarks 71

List of Tables

Table 2.1: F-test for difference in variances of peak discharge of Mekong River at Kratie, Cambodia between two time periods. 12

Table 3.1: Agreement of MODIS NDVI change flood detection product compared to Landsat RGB 742 (P/R: 126/52) displays during the 2006 flood season. 37

Table 3.2: Agreement of MODIS NDVI change flood detection product compared to Landsat RGB 742 and ISERV true color imagery during the 2013 flood season. 37

Table 5.1: Impact estimates of 2011 flood in Cambodia compared to NGO reports. 66

Table 5.2: Impact estimates of 2013 flood in Cambodia compared to public reports. 67

List of Figures

Figure 1.1: Maps of the Mekong Basin: River network (left); Topography (middle); and main catchments in the Lower Mekong Basin (right) (from Naeimi et al. 2013). 3

Figure 1.2: Daily mean discharge of Mekong River at Kratie, Cambodia, from 1985-2008. 4

Figure 1.3: Mean annual runoff of Lower Mekong Basin (MRC, 2010). 5

Figure 2.1: Location of Kratie stream gauge and and topography of southern region of the Lower Mekong Basin (left). Flood extent in October, 2011, darker red indicates more severe flooding (see chapter 3). 9

Figure 2.2: Peak discharge of Mekong River at Kratie, Cambodia from 1924 – 1970 and1985-2008. Years 1971- 1984 were missing from the dataset. ..11

Figure 2.3: Location of US bombings in Cambodia 1965 – 1973 in purple (Cambodia Mine Action and Victim Assistance Authority (CMAA)).13

Figure 2.4: Calculated recurrence interval of annual peak discharge values of Mekong River at Kratie, Cambodia of years a.) 1924-1970 b.)1985-2009, and c.) all years together. A logarithmic regression was fit to each dataset (black line).....15

Figure 2.5: Annual flood recurrence interval of Mekong River at Kratie, Cambodia for years 1924-1970 and 1985-2008.....16

Figure 2.6: Start date of flood season of Mekong River at Kratie, Cambodia for years 1924-1970 and 1985-2008. 17

Figure 2.7: End date of flood season of Mekong River at Kratie, Cambodia for years 1924-1970 and 1985-2008.....18

Figure 2.8: Length of flood season of Mekong River at Kratie, Cambodia for years 1924-1970 and 1985-2008.....18

Figure 3.1: Time-series of Terra MODIS-derived NDVI from a rice paddy (green), mean daily river discharge (blue) from 1985-2008 of the Mekong River at Kratie, Cambodia. The effect of the seasonal flooding over the pixel is evident from the dynamic range of NDVI and river discharge climatology. The Mekong River Commission provided the river discharge data. 25

Figure 3.2: Data processing framework used to produce NDVI-based flood impact product from single-satellite MODIS flood scene image.....29

Figure 3.3: Comparison of MODIS derived flood map with SAR map for October 2011 event. 33

Figure 3.4: Comparison of MODIS derived flood map with SAR map for October 2013 event. 35

Figure 3.5. Landsat scenes (bottom) used for validation of the corresponding MODIS NDVI change product (top) of the region surrounding Phnom Penh, Cambodia. Landsat scenes (Path/Row 126/52) are displayed in false color RGB 742. (Date 1) MODIS NDVI change product from 8 day composite acquired 8/29 – 9/5/2006; Landsat 5 TM acquired 9/3/2006. (Date 2) MODIS NDVI change product from 8 day composite acquired 10/16 – 10/23/2006; Landsat 5 TM acquired 10/21/2006. (Date 3) MODIS NDVI change product from 8 day composite acquired 11/1 – 11/8/2006; Landsat 5 TM acquired 11/6/2006. 36

Figure 3.6: Comparison of inundation product from 8-day composite starting 11/1/2013 (right; overlain on ISERV) with ISERV natural color imagery (middle) and Landsat 7 ETM+ false color (RGB 742; left) from 11/1/2013 demonstrates degree of flooding and partially flooded pixels represented by the amount of decrease in NDVI.....40

Figure 4.1. Location of areas suitable for different rice cultivation strategies (top) and percent of communes that are covered by rice paddies (bottom) in Cambodia.....46

Figure 4.2: Average NDVI values from MODIS 250-m data for different land cover types defined by MODIS Land Cover Classification product (MCD12Q1) (From Fayne et al. 2017).....47

Figure 4.3: Wet season hydrographs of Mekong River at Kratie, Phnom Penh, and Tan Chau in Cambodia. 2011 flood and other events on the left, and the 2015 drought shown on the right. Graphs acquired from Mekong River Commission. 49

Figure 4.4. Mean NDVI (top) and standard deviation of NDVI (bottom) of the study area on October 16 for the years 2005-2014. 51

Figure 4.5. Flood extent on October 16, 2011 overlain on the standard score for that date compared to average conditions for this period for the years 2005-2014 (top) and the z-score for 10/16/2011 compared to the historical statistics (bottom). 53

Figure 4.6: Flood extent on October 16, 2015 overlain on the standard score for that date compared to average conditions for this period for the years 2005-2014 (top) and the z-score for 10/16/2011 compared to the historical statistics (bottom). 55

Figure 5.1: Study area of Cambodia, outlined in magenta. 60
Figure 5.2: Flood extent derived from 8-day MODIS composite from October 16, 2011. 61
Figure 5.3: People per 100m x 100m pixel in Cambodia acquired from WorldPop (www.worldpop.org.uk) 62
Figure 5.4: User-defined input parameters for flood impact estimation tool. 64
Figure 5.5: Results of intersection between flood map and population data, and attribute table with calculations of people affected in each polygon.65
Figure 5.6: Number of people affected by 2011 flood in Cambodia in each 100m x 100m pixel. 68
Figure 5.7: Total number of people affected by 2011 flood by province.....69

Chapter 1: Introduction

The sixty million inhabitants of the Lower Mekong River Basin (LMB) in Southeast Asia and a remarkably diverse aquatic ecology and fishery (Ziv et al. 2012) rely on the natural resources provided by the Mekong River and its annual flooding. The river and its seasonal flood pulse drives the productivity of agriculture and fisheries, which supports the well-being, ecosystems, and the economy of the region (Dugan, Delaporte, Andrew, O'Keefe, & Welcomme, 2010; Mekong River Commission (MRC), 2009). For hundreds of years, however, the people of the region have also had to cope with extreme floods and droughts with changes in the Asian Monsoon and movement of the ITCZ (Buckley, Fletcher, Wang, & Zottoli, 2014). Recent extreme flood events, such as in 2013 and 2011, affected millions of people, claimed many lives, and caused millions of dollars of damage to infrastructure and agriculture (MRC, 2015).

Long-term monitoring of the Mekong River can help resource managers understand risk and respond to flood disasters. *In-situ* monitoring of the river provides valuable information on the intensity and history of flooding. But, these methods, such as stream gauge stations, have limited use for understanding the spatial distribution of flooding and responding to disasters. Satellite remote sensing and Geographic Information Systems (GIS) are state-of-the-art technologies that can be used for understanding spatial flood risk and damage of flooding, and can help direct resources to respond to flood disasters. In this paper, I aim to use stream gauge data, remote sensing data, and GIS to understand historical flood patterns and provide tools to monitor and respond to disaster events. First, I use historical gauge information to evaluate changes in peak discharge and timing of annual flooding. Next, I develop a method for mapping floods and relative intensity using satellite remote sensing. Lastly, I provide an ArcGIS

Toolbox to evaluate potential socio-economic damage from flood disasters. By combining *in-situ* data with space-based measurements and geo-spatial technologies, we can understand changes in annual flooding through time and provide tools to evaluate and respond to flood disasters in the LMB.

STUDY AREA

The Mekong River is the largest international river in Southeast Asia, starting at its headwaters in China, flowing through Myanmar, Laos, Thailand, Cambodia, and Vietnam (Figure 1.1). The river is the world's 12th longest, and 8th largest in terms of discharge. Despite a long history of human occupation, the Mekong has remained relatively pristine until recently, with the largest inland fishery on the planet and one of the world's most bio-diverse rivers, second to the Amazon (Ziv et al. 2012; Mekong River Commission (MRC) 2011). In addition, the southern part of the LMB is also one of the region's major rice producers, primarily in Cambodia and the Vietnam Delta (Mekong River Commission (MRC), 2011).

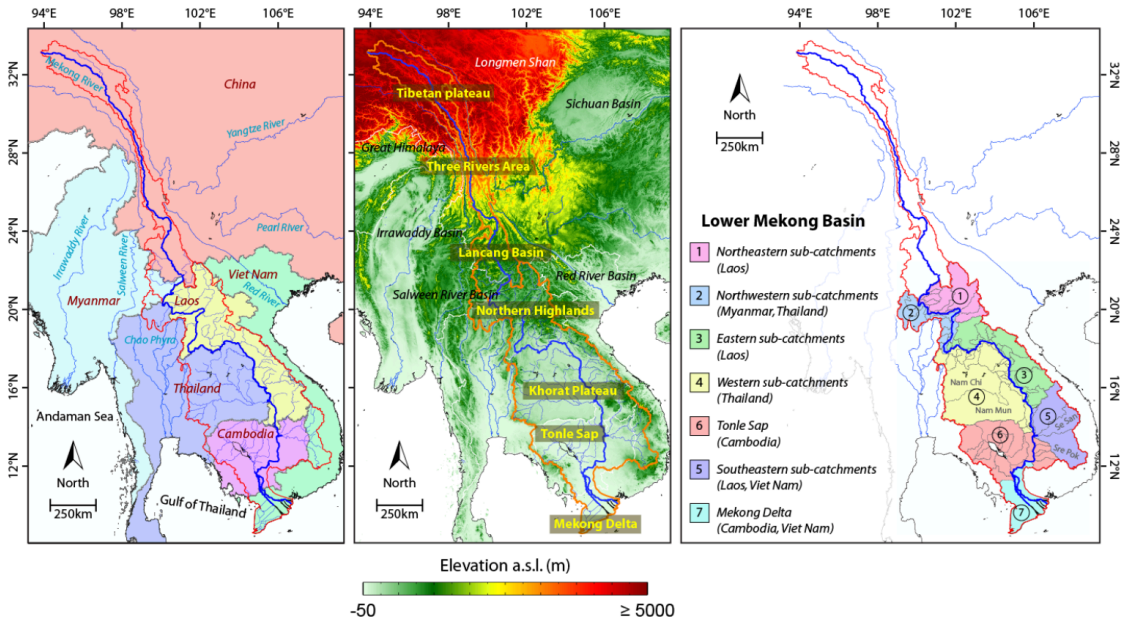

Figure 1.1: Maps of the Mekong Basin: River network (left); Topography (middle); and main catchments in the Lower Mekong Basin (right) (from Naeimi et al. 2013).

Natural riparian ecosystems of the LMB has coevolved with intensive seasonal flooding. The area is climatically driven by the Asian Monsoon, which results in large dynamic wet and dry seasons of almost equal length. The highest rainfall occurs in July, August, and September in most of the basin; however, there is a slight shift to a later wet season in Cambodia and the delta region, where September and October are the wettest months. In fact, roughly 75% of the annual discharge occurs during the wet season from July through October (Brunier, Anthony, Goichot, Provansal, & Dussouillez, 2014) (Figure 1.2). The majority of the water comprising the annual floods originates in upland areas of the basin, mostly in Laos (Figure 1.3). The water accumulates upstream and spreads out into the floodplain when it reaches the Tonle Sap Catchment (Figure 1.1). During the wet season, excessive water volumes flow backward up the river into Tonle Sap Lake (Mekong River Commission (MRC), 2011). The area of Tonle Sap Lake

becomes 3-6 times larger during the wet season than during the dry season. The water stored in the lake during the rainy season discharges during the dry season, providing water for the local communities year round.

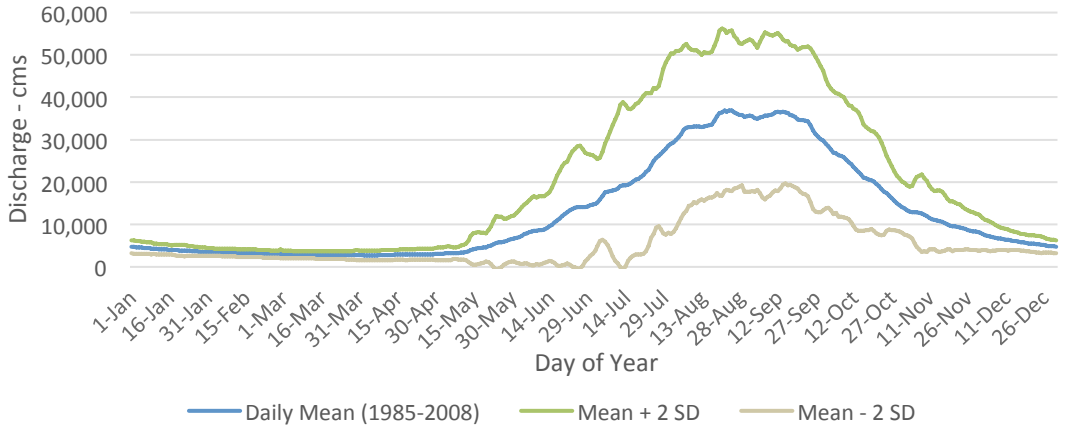

Figure 1.2: Daily mean discharge of Mekong River at Kratie, Cambodia, from 1985-2008.

The seasonal flood pulse of the Mekong drives the dynamics of the natural ecosystems, and supports the expansive agriculture throughout the Cambodian floodplain and the Mekong Delta in Vietnam. The LMB supports over 10 million hectares of rice agriculture alone, which has replaced extensive tracts of natural wetlands and forests (ICEM, 2013). The seasonal flood pulse, therefore, is essential to support the high biodiversity and natural systems of the region, as well as the health and livelihood of the people and the economy of the countries of the LMB. Flooding in the region, however, has also periodically caused significant losses of human life and damaged property, agriculture, and infrastructure (IPCC, 2014; Mekong River Commission (MRC), 2012).

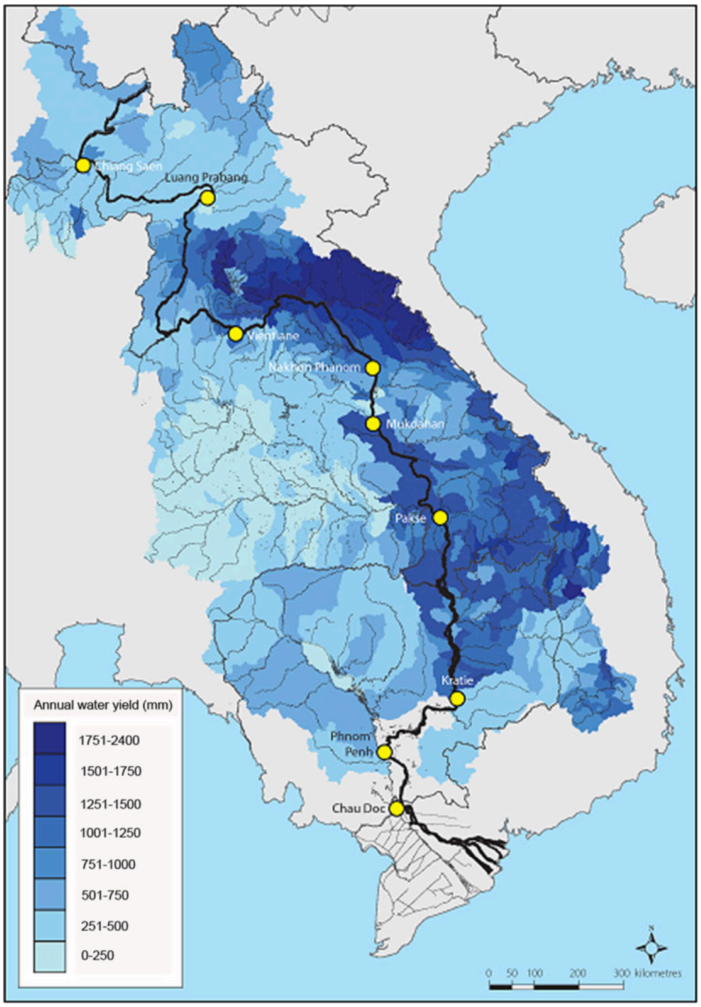

Figure 1.3: Mean annual runoff of Lower Mekong Basin (MRC, 2010).

Recent studies have estimated that annual losses from flooding in the LMB are $60-70 million annually. In contrast, economic gain from flooding due to nutrient replenishment and fish habitat is ~$8-10 billion annually (Mekong River Commission (MRC), 2012). Proper flood management is essential for maintaining the livelihoods and economy of the LMB. The effects of severe flood damage in this region can even affect global communities and markets. Thailand and Vietnam produced 51% of the world's rice exports in 2008, mostly in the LMB (Mainuddin, Kirby, & Hoanh, 2011), and the

Mekong contains the world's largest freshwater capture fishery (Mekong River Commission (MRC), 2011). Intensified floods and droughts caused nearly 90% of rice production losses in Cambodia during 1996-2001 (MRC, 2009). Future climate change may only increase the occurrence and severity of flood damage in this vulnerable area.

Over the past 30-50 years, Southeast Asia has experienced several aspects of climate change, including an increase in temperature, an increase in rainfall during the wet season, and decreases during the dry season, intensified flood and drought events, and sea-level rise (IPCC, 2014). The effects of climate change on the discharge and flood frequency, however, are still not fully understood. Uncertainty in climate models changes the effects of climate change scenarios on the amplitude and timing of the flood season (Thompson, Green, & Kingston, 2014; Thompson, Green, Kingston, & Gosling, 2013). For example, different estimations of potential evapotranspiration (PET) parameters significantly change the results of discharge estimates for various climate models, because PET estimates influence precipitation estimates (Thompson et al., 2014, 2013). In addition, Thompson et al. (2013) note that climate models have 2.5 to 6 times more uncertainty than the hydrologic models. Models have suggested different effects of climate change in different parts of the basin, with estimations of increased precipitation in upper parts of the basin and reductions downstream (Thompson et al., 2013). Further limiting the ability to observe spatiotemporal changes in the climate and seasonal floods is a simple lack of meteorological data (Piman, 2014). Understanding historic changes in the annual flooding, however, is key to understanding the effects of climate change and human activity and for predicting future scenarios.

Chapter 2: Recent Changes in Annual Flooding

INTRODUCTION

The MRC estimated that 1.2 million people around Tonle Sap Lake are fishers and farmers who depend on the floods. The lake and river provide 75% of the country's inland fish and is the main source of protein for the Cambodian people. The timing and extent of the annual floods, however, have a major impact on fish productivity (Mekong River Commission (MRC), 2010). Relationships between annual flood volume and peak discharge are not directly linear, however, so the long-term trends in the annual flooding are not clear (Dung, Merz, Bárdossy, & Apel, 2015). But, climate change models show a likely shift in the start of the flood season (Thompson et al., 2013). Over the last several centuries at least, societies have adapted to or suffered from changes and extremes in the Asian Monsoon and the annual flooding of the Mekong (Buckley et al., 2014). Although these extreme events will continue in the future, anthropogenic management of the river will have immediate effects, both positive and negative.

Land use change and the development of hydropower in the LMB is expected to alter the flow and annual flood pulse of the river (Arias et al., 2012, 2014; Kite, 2001; Kuenzer, Campbell, et al., 2013; Lu, Li, Kummu, Padawangi, & Wang, 2014). Recent hydropower development has had many effects on the floodplain system, and there are many more dams in the being planned. The construction of dams in China may have reduced flow of the river through the northern reaches of the LMB (Lu et al., 2014). Hydropower dams also reduce sedimentation in the floodplain in Cambodia and the Vietnam Delta, which is the source of nutrients and soil aggradation (Thompson et al., 2013). These effects on the geomorphology and hydrology of the basin will potentially have negative effects on habitat cover, sedimentation, and net primary productivity (NPP) of Tonle Sap Lake and surrounding ecosystems. Thompson et al. (2013) expect these

effects of hydropower development combined with climate change to cause a decline in ecosystem services provided by the Mekong River and seasonal flooding.

In order to appropriately respond to both climate-driven and anthropogenic-driven changes in annual flooding, we must first understand what changes are occurring. People and industry may be affected differently by different types of changes in the seasonal flooding of the Mekong. For this study, I chose to focus on peak discharge as a measure of annual flood magnitude to identify extreme events, and the timing and length of the flood season because of its importance to agricultural production. I investigate the temporal changes in seasonal flooding of the Lower Mekong Basin by addressing 4 questions:

How has the magnitude of flooding changed over recent history?

How has the frequency of large floods changed?

Has the timing of the flood season changed?

Are these changes driven by climatic or anthropogenic forces?

METHODOLOGY

We acquired stream gauge data for several stations from the Mekong River Commission. The gauge on the Mekong at Kratie was used for the analysis because it is frequently used as a benchmark for the system and had a longer and more complete record than most of the stations (Figure 2.1). The dataset includes daily average discharge measurements from 1924-1970, and 1985-2008, with missing data from 1971-1984. Peak discharge was determined for each year as a measure of annual flood magnitude.

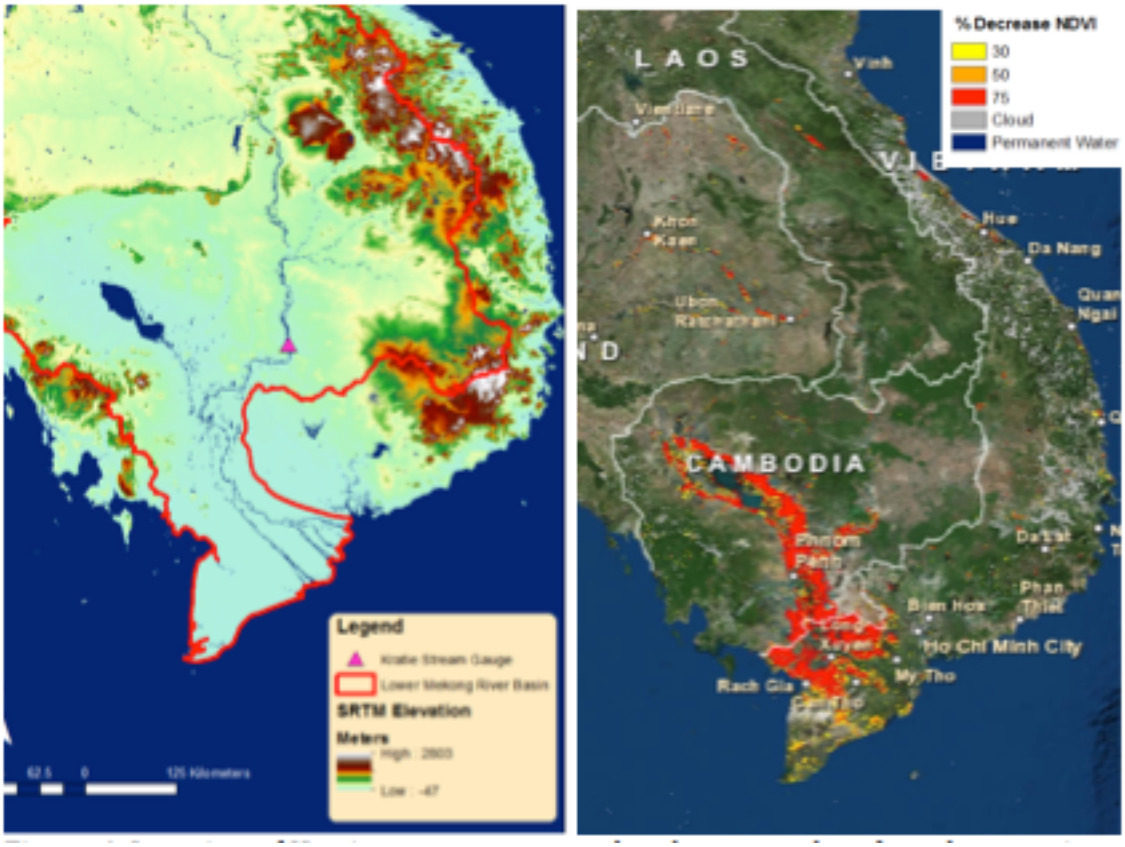

Figure 2.1: Location of Kratie stream gauge and topography of southern region of the Lower Mekong Basin (left). Flood extent in October, 2011, darker red indicates more severe flooding (see chapter 3).

I analyzed the time series of peak discharge for long-term trends in the annual flood magnitude using linear regression. First I analyzed the two time periods (1924-1970, 1985-2008) separately, then as a continuous dataset. I applied a student t-test to determine statistical significance of the trends. Then I used an F-test to determine the difference in variance of the annual flood magnitudes between the two time periods.

Next, I calculated the probability of occurrence and the recurrence interval for the annual flood peaks. I determined the probability of occurrence for each annual peak discharge in the Kratie record using the equation

$$P = 100 \times (m/(n+1))$$

where P is probability, m is the rank of the peak discharge with 1 being the largest discharge through n, the number of flood events. I converted the probability of each event into recurrence intervals with the equation

$$R = 100/P$$

where P is the probability and R is the recurrence interval, the average amount of time for a flood of the same magnitude to occur. Again, I analyzed each time period separately and then together. I was then able to observe trends in the frequency of high magnitude events through time.

Lastly, I investigated trends in the timing of the flood season. The beginning of the flood season in the LMB is defined as when the river discharge rises above the long-term mean. The end of the flood season is determined by the down crossing of the discharge past the historical mean. Generally, there is only one up crossing and down crossing date, but when more than one, the earliest date was used for the start, and the latest date used for the end of the flood season. At Kratie, the mean used for defining the flood season is 13,600 m^3 sec^{-1}. I then used a linear regression and t-test of significance to investigate changes in the timing and length of the flood season. An F-test determined differences in the variability of the timing of the flood season.

RESULTS AND DISCUSSION

Trends in Peak Discharge

There is not a siginificant directional trend in the peak discharge record from Kratie station for either time periods (1924-1970 and 1985-2008) separately or as a whole (Figure 2.2).

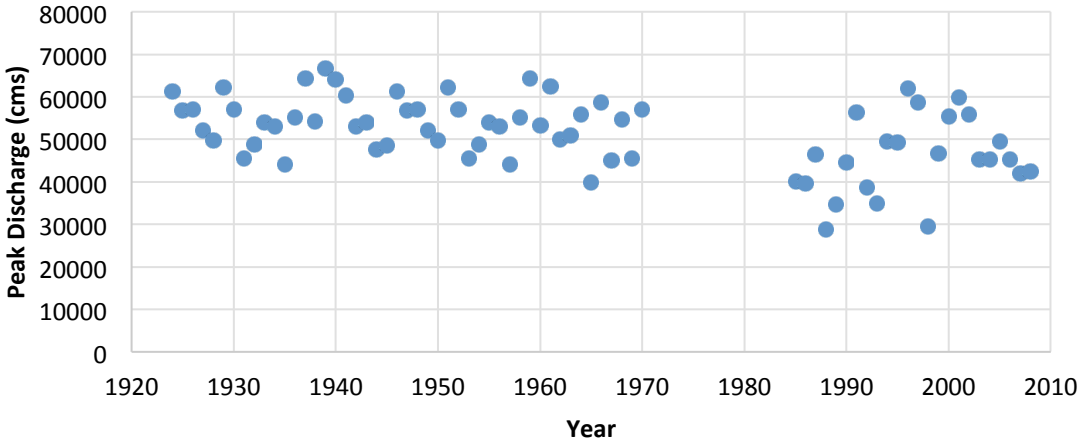

Figure 2.2: Peak discharge of Mekong River at Kratie, Cambodia from 1924 – 1970 and1985-2008. Years 1971- 1984 were missing from the dataset.

Although there is no directional trend in the peak discharge since 1924, the variability in peak discharge was significantly higher in the second time period (1985-2008) than in the first time period (Table 2.1). The precipitation from the Kratie station had too many missing data values to provide an accurate assessment of precipitation trends during the study period. Other studies, however, have shown that temperature has been increasing since 1970 in the region, but how these values compare to historical means and fluctuations remains to be assessed for the entire study period (Zhou et al., 2006). In addition, Räsänen and Kummu (2013) have shown that changes between El Nino and La Nina have have a strong correlation with peak discharge during much of the

study period, but there is still no strong explanation for the variability of peak discharge. The spatiotemporal patterns of the monsoon have an effect on the annual peak discharge of the river, but hydropower development and land cover change have a stronger impact on the seasonal flood dynamics (Arias et al., 2014). These observations raise many questions as to the driver of the increase in variability of the flood peaks between the two time periods.

Table 2.1: F-test for difference in variances of peak discharge of Mekong River at Kratie, Cambodia between two time periods.

	1985-2008	1924-1970
Mean	45888.75	54119.8021
Variance	83295976.4	38944596.3
Observations	24	47
df	23	46
F	2.13883271	
P(F<=f) one-tail	0.014051	
F Critical one-tail	1.76680532	

The historical context of the region may give insight into changes in the landscape that could lead to changes in the hydrologic cycle during the period of data gap, 1971-1984. During the 1970s, the Vietnam War and the civil war in Cambodia devastated much of the landscape. Among the widespread damage, US alone bombed a large portion of the country (Figure 2.3). Additionally, land was being converted for agriculture under the reigning communist government at the time. All of these changes in the basin likely led to widespread forest decline, and change in the geomorphic systems. Deforestation has continued and even increased in recent years (Leinenkugel, Wolters, Oppelt, & Kuenzer, 2015). This deforestation comes from multiple causes and could lead to an

increase in watershed response to precipitation events (Zhang & Werner, 2015). Certainly, we need more data to precisely determine the contribution of climate change, land use change and destruction, and hydropower development to the increase in variability of the annual flood peak between the two time periods.

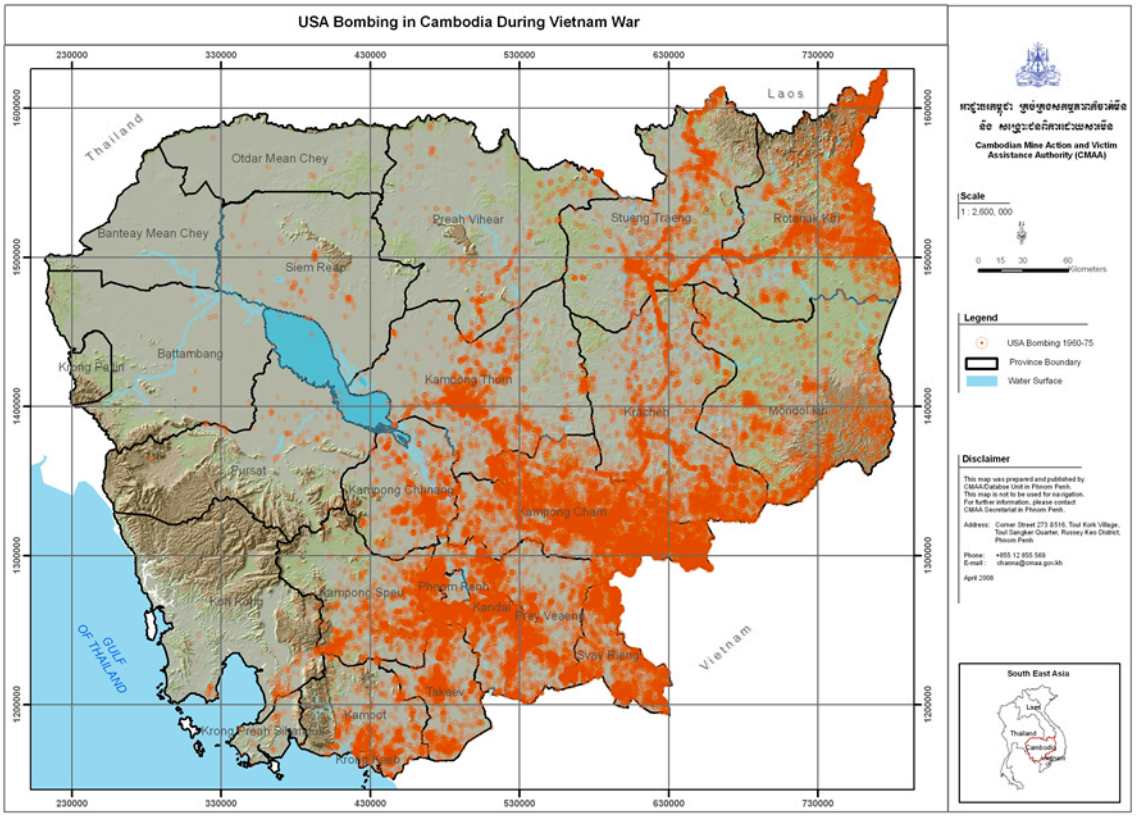

Figure 2.3: Location of US bombings in Cambodia 1965 – 1973 in purple (Cambodia Mine Action and Victim Assistance Authority (CMAA)).

Flood Recurrence

The flood recurrence interval for discharges calculated during the study period was heavily dependent upon the length of the data record, and time period used (Figure 2.4). The number of years of a recurrence interval for various discharges was greatly different depending on which time series was used. For example, the largest (least frequent) peak discharge during 1924-1970 was 66,700 m^3/sec. This flood magnitude,

which occurred in 1939, had a recurrence interval of 48 years. When combined with the second time period as well, however, this discharge had a return interval of 72 years. The peak discharge from 1985-2008, 61,938 m^3/sec, occurred in 1996 and had a recurrence interval of 25 years. When combined with the first time period, however, this discharge had a recurrence interval of 9 years. Depending on the length of your data set used to calculate the probability of occurrence, a discharge value could have a drastically different recurrence interval. These results are important for understanding the appropriate calculation and use of flood recurrence intervals. Because the probabilities are entirely dependent upon the length of the record, it is important not to extrapolate beyond the length of the record. Instead of always normalizing to 100 years as calculated in this study, probabilities should only be normalized to the length of the record used to calculate probabilities.

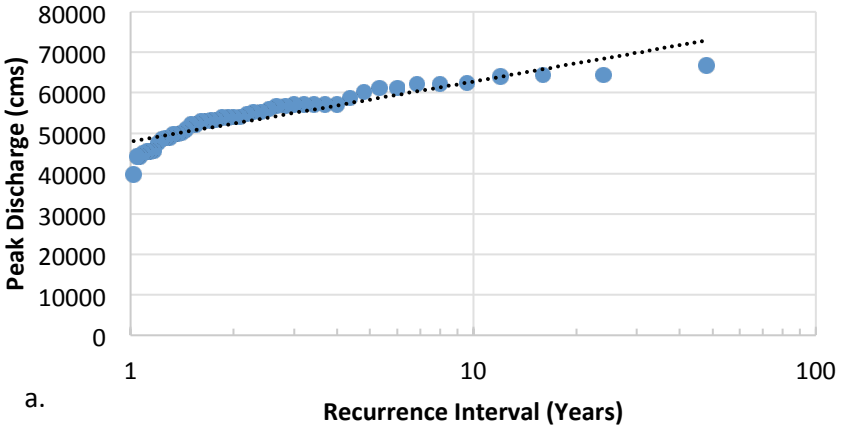

a.

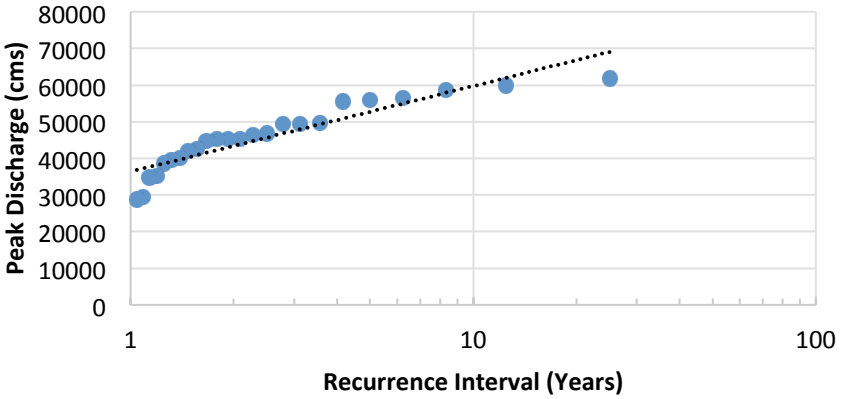

b.

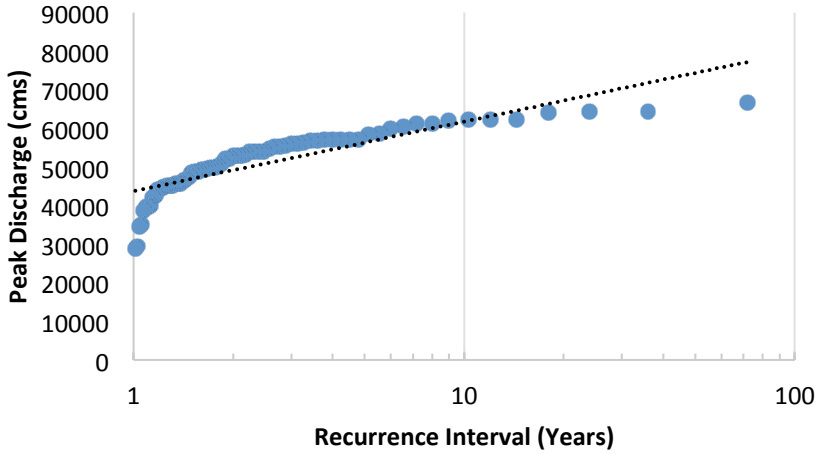

c.

Figure 2.4: Calculated recurrence interval of annual peak discharge values of Mekong River at Kratie, Cambodia of years a.) 1924-1970, b.)1985-2009, and c.) all years together. Each dataset has a base 10 logarithmic regression (black line).

Some climate change models predict the increase in frequency of extreme events in this region (IPCC, 2014). The available data for years 1924-2008, however, does not seem to indicate any increase in the frequency of larger flood events (Figure 2.5). In fact, a qualitative analysis suggests that there were more large-magnitude floods during the earlier time period than more recently. I cannot draw direct conclusions from this data,

but these larger floods could be just from natural variation, or increased management of the river has reduced extreme discharges downstream.

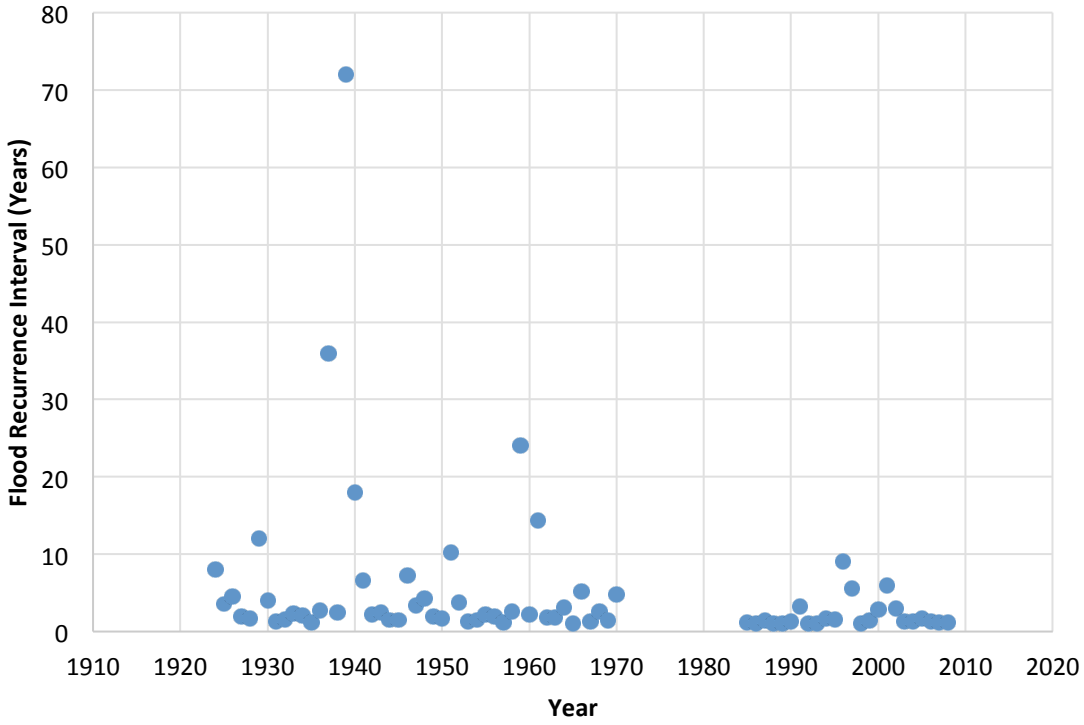

Figure 2.5: Annual flood recurrence interval of Mekong River at Kratie, Cambodia for years 1924-1970 and 1985-2008.

Timing and Length of Flood Season

There does not seem to be a directional trend in the change of the start date of the flood season (Figure 2.6). It appears, however, that there may be more variability in the start date of the flood season. More data and further statistical analyses are needed to determine the significance of this observation. Variability in the start date of the flood season, however, could have effects on fish productivity of the river and Tonle Sap Lake. In addition, less predictability in the onset of the flood season makes it difficult to appropriately plan planting schedules. There does not seem to be significant changes in

the end date or length of the flood season in this dataset (Figure 2.7, Figure 2.8). The length of the flood season is slightly more variable in more recent years because of the start dates of the season. The general consistency in length of flood season is good for the continued productivity of the ecosystems and agriculture that depend on the long-term regularity of the seasonal floods.

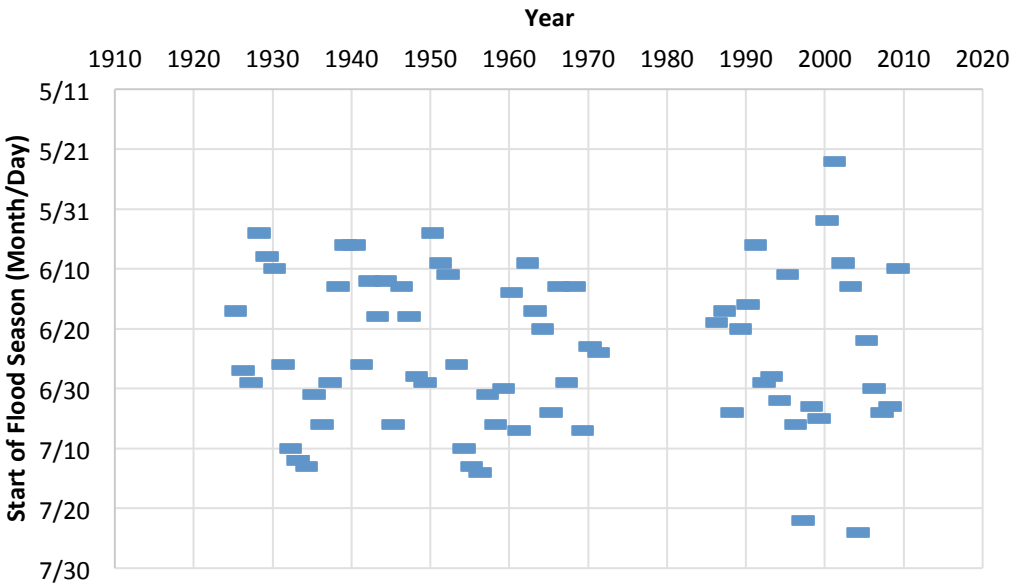

Figure 2.6: Start date of flood season of Mekong River at Kratie, Cambodia for years 1924-1970 and 1985-2008.

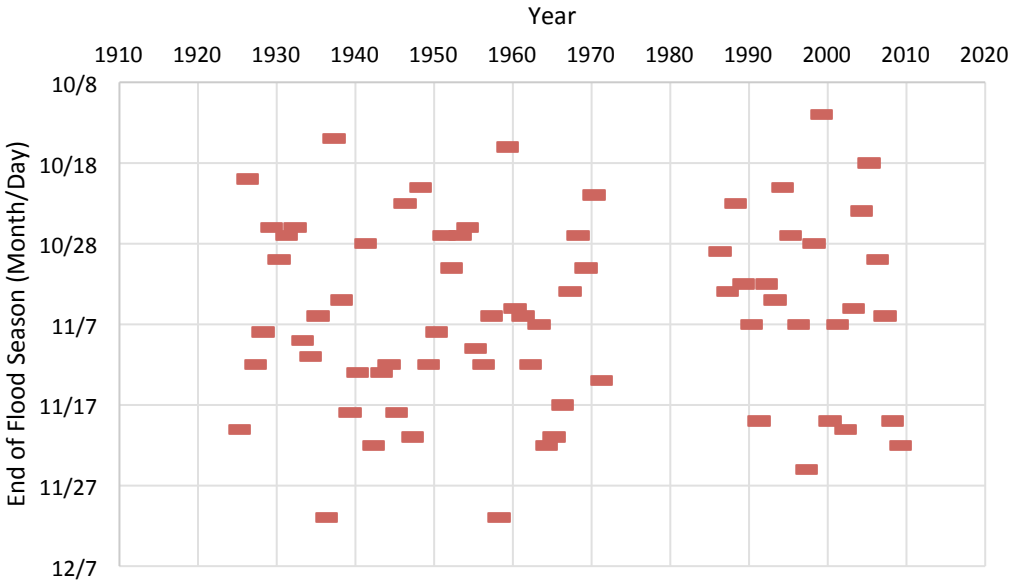

Figure 2.7: End date of flood season of Mekong River at Kratie, Cambodia for years 1924-1970 and 1985-2008.

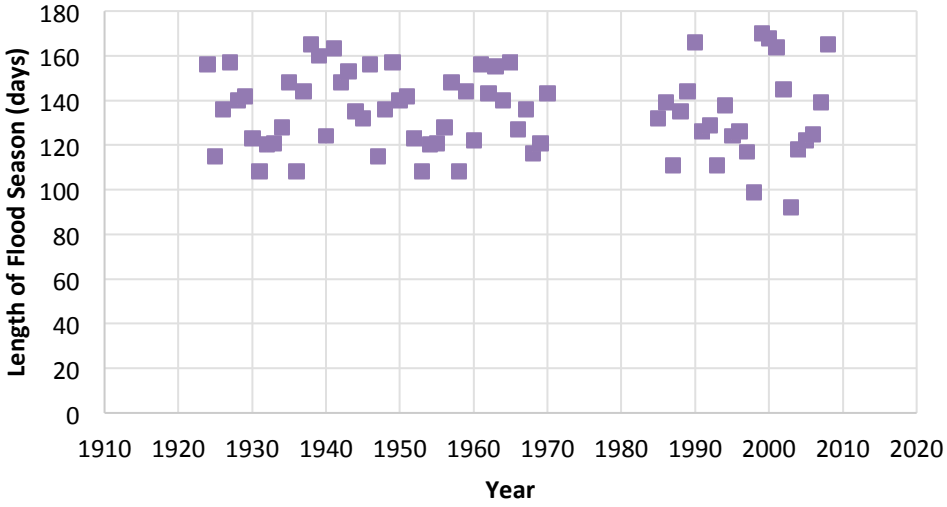

Figure 2.8: Length of flood season of Mekong River at Kratie, Cambodia for years 1924-1970 and 1985-2008.

CONCLUSIONS

The Lower Mekong River Basin, and particularly Cambodia and the Vietnam Delta, is very susceptible to climate change, upstream hydropower development, and land use change. People in this region are particularly vulnerable to changes in the annual flood dynamics of the Mekong River, because their livelihoods depend directly upon it. This region is rapidly developing, and recent changes have decreased sedimentation and flow rates of the river downstream. To understand the potential future effects of the projected development and continued land cover change and climate change, it is important to understand how the flood regime is changing in relation to historical context.

The large gap in the datasets were limiting to the types of analysis and conclusions to be made in this study. Regardless, I can conclude that the variability of the peak flood discharge has increased in recent years compared to the long-term trend before 1970. Although it is difficult to distinguish contributing factors to this observation, it is likely that deforestation and land use change that occurred during the years of missing data, 1970-1985, had an influence on response of the watershed to precipitation events. Much more data are needed, however, to determine the primary driver of this trend. In addition, despite projected increases in extreme events in the region with increasing global warming, these data showed an increase of rare flood events in 1924-1975 over 1985-2008, regardless of the difference in length of records. There are too few precipitation data to determine if precipitation or flood control measures caused the decrease of rare events in the more recent period. Describing floods in terms of recurrence intervals based on peak flood discharges, however, may not be accurate for comparing events. The calculated recurrence time is very heavily dependent upon the time period and length of the record used for calculations. Probabilities of events, therefore, should not be converted to return intervals beyond the length of the record

because the records are period dependent and probably will become more so with increasing global warming (IPCC).

Lastly, there does not seem to be a trend in changes of the timing or length of the flood season, but it is possible the start date of the flood season is becoming more variable. More investigation is needed to determine significant trends, and numerous factors could contribute to this observation. With increased hydropower development along the Mekong, it will be important to manage the river to maintain the timing and length of the downstream flooding for agriculture and fisheries while adapting to changes in the monsoon.

The Lower Mekong River Basin is an extremely bio-diverse region where millions of people live with and depend upon the regular seasonal flooding of the Mekong River. The magnitude of the floods affects people and infrastructure directly and indirectly, but the timing and length of the floods can have effects on the fishery and agricultural productivity of the region as well. With increasing development and projected climate change threatening the ecosystem services of the Mekong that sustain millions of livelihoods, it is vital to monitor annual flood trends in relation to historic patterns.

Chapter 3: Monitoring Mekong Flooding from Space

INTRODUCTION

Like many tropical regions, the Lower Mekong River Basin (LMB) is vulnerable to seasonal flooding, which produces the normal flow regime ecology but can pose negative and positive impacts on local communities. Floodwaters carry nutrient-rich sediment that deposits as the floods recede, naturally replenishing and fertilizing the soils of the floodplain for sustaining agricultural production, and providing habitat for fish and various aquatic and terrestrial animals (Kuenzer, Campbell, et al., 2013). During extreme events, however, large floods can lead to loss of life, cause damage to infrastructure, and threaten the availability of natural resources. As climate change and development continues to intensify flood risk and associated damage to agricultural output and urban areas, there is a need for transboundary coordination of flood monitoring and risk management planning (IPCC, 2014). This has led to an increased need to develop rapid response tools that can support developing viable climate change adaptation policy and bridging the gap between scientific and community-based knowledge (IPCC, 2014). Synoptically measuring floods *in situ*, however, is generally very difficult and time consuming, but utilizing space-borne and airborne observations provides a realistic method for consistent and rapid wall-to-wall monitoring of large flood events through time (Kussul, Shelestov, & Skakun, 2011). This study attempts to create a historical and near real-time flood monitoring system for the LMB using Moderate Resolution Imaging Spectroradiometer (MODIS) satellite data in order to help respond to these devastating flood events and assess damage.

Previously published flood mapping efforts in the LMB included a variety of sensors to observe temporal changes in inundation extent and frequency to understand the dynamics of historical seasonal flooding (Boschetti, Nutini, Manfron, Brivio, & Nelson,

2014; Hostache, Matgen, & Wagner, 2012; Klein et al., 2015; Kuenzer, Guo, et al., 2013; Nguyen Thanh Long, 2001; Sakamoto et al., 2007; Son, Chen, Chen, & Chang, 2013). Radar, Landsat, and MODIS time-series data have all proved to be conditionally useful for remote sensing of floods, but all have advantages and limitations depending on the application and data processing technique (Kuenzer, Guo, et al., 2013; Nguyen Thanh Long, 2001; Sakamoto et al., 2007). For example, radar sensors can effectively penetrate clouds, which are a major issue for electro-optical remote sensing in the tropics. Multi-temporal radar images can be used to detect changes in the surface due to flooding without the impacts that atmospheric contamination poses to optical data (Nguyen Thanh Long, 2001). The sparse acquisition frequency, reduced data availability, and data processing requirements for radar data, however, make such data less advantageous for many rapid disaster assessments or continuous monitoring. Landsat data provide high spatial and spectral resolutions, but the return time renders cloud obstruction an issue in many parts of the world. In the tropics, cloud coverage can be frequent and heavy (Asner, 2001), which presents a major challenge for viewing floods with an optical sensor, and false water detection can be caused by cloud and cloud shadows. The MODIS sensor on board the Aqua and Terra satellites provides two images a day, with many spectral bands ranging in resolutions of 250-m, 500-m, and 1 km. Although at a coarser spatial resolution, MODIS provides frequent acquisitions that allow for temporal compositing to remove cloud obstruction, and for continuous and rapid regional flood monitoring applications (Brakenridge & Anderson, 2006; Klein et al., 2015; Sakamoto et al., 2007).

Several studies have demonstrated utilizing MODIS products for analyzing temporal dynamics of inundation in the region (Klein et al., 2014; Kuenzer, Guo, et al., 2013; Sakamoto et al., 2007). Sakamoto et al. (2007) used thresholds on EVI, LSWI, and the difference between the two indices to estimate flooded, mixed flooded and not

flooded, and not flooded pixels. Klein et al. (2015) demonstrated the use of a dynamic threshold based on standard deviations from permanent water body values to identify water body dynamics on a global scale. The Near Real-time Global Flood Mapping Project, which uses MODIS near real-time 250 m red and near infrared data to detect surface water using an algorithm originally developed for the Dartmouth Flood Observatory (DFO) (Nigro, Slayback, Policelli, & Brakenridge, 2014). The DFO algorithm is used to produce a global surface water product, which then removes perennial water to map surface floodwater. Assessing the accuracy of this product on a global scale is still ongoing (Nigro et al., 2014). Additionally, many normalized spectral indices have been developed and tested for detecting surface water at different MODIS resolutions, but all require manual thresholds that can be region or scene dependent (Boschetti et al., 2014; Huang, Chen, & Wu, 2014; Ji, Zhang, & Wylie, 2009; Son et al., 2013; Sun, Yu, & Goldberg, 2011; Tornos et al., 2015). All of these methods can be used to detect surface water extent, but none give insight into the degree of flooding or impact, and may have difficulty with mixed pixels, particularly in flooded rice agriculture (Boschetti et al., 2014).

In response, I assess a novel use of MODIS Normalized Difference Vegetation Index (NDVI) to detect regionally evident flood inundation in the LMB, and to derive information on the relative degree of flooding. Vegetation changes from flooding can be detected and monitored using multiple dates of NDVI derived from satellite-based cloud-free multispectral data. NDVI's native scaling ranges from -1 to +1. Dense vegetation has NDVI values close to 1, while water tends to have negative NDVI values (Domenikiotis, Loukas, & Dalezios, 2003; Fayne et al., 2017; Sanyal & Lu, 2004). Using a threshold on NDVI values can reliably detect surface water, but a single threshold does not work in different regions, or even through time. Comparing NDVI values over flooded areas to a

non-flooded baseline show that inundated areas have a significant decrease in NDVI compared to the non-flooded baseline NDVI. Multi-date image change detection methods have successfully been employed with MODIS data to detect forest defoliation (Spruce et al., 2011), fires, and floods (Domenikiotis et al., 2003). Because NDVI is sensitive to underwater bottom characteristics in rice paddies (Boschetti et al., 2014), this approach can also give insight into the degree of flooding in the region to help assess impacts and mixed pixels. To this end, the current study aims to produce a flood inundation product that can give insight into the degree of flooding on a rapid or near-real time basis, maximizing utility for disaster and agricultural assessment applications for the LMB. Although the methods in this paper are applied to the entire LMB, I focus validation on Cambodia, where there is a strong dependence on flooding for fish and rice agriculture.

METHODOLOGY

Flood Detection

Here we employ a MODIS NDVI-based algorithm and inundation-mapping tool to evaluate land surface changes due to flooding. We custom developed this algorithm for the largely tropical LMB, which contains distinct dry and wet seasons. It compares NDVI from the wet season to that from the dry season to identify areas with reduced NDVI due to flooding (Figure 3.1). When a surface feature is inundated, its NDVI value will change significantly (Sanyal and Lu 2004). Calculating the percent change in NDVI between a wet season flood event and a dry season historical baseline reveals the relative degree of flooding (either currently or recently flooded). This method can be readily applied to the study area because although intensity of precipitation and flooding may change from year to year during the wet season, there remains little variation during the dry season, and the

duration of the distinct seasons is consistent through time (Figure 3.1). This seasonality allows us to generate a dry season historical baseline to use as reference values for non-flooded conditions, in order to detect inundation during the wet season.

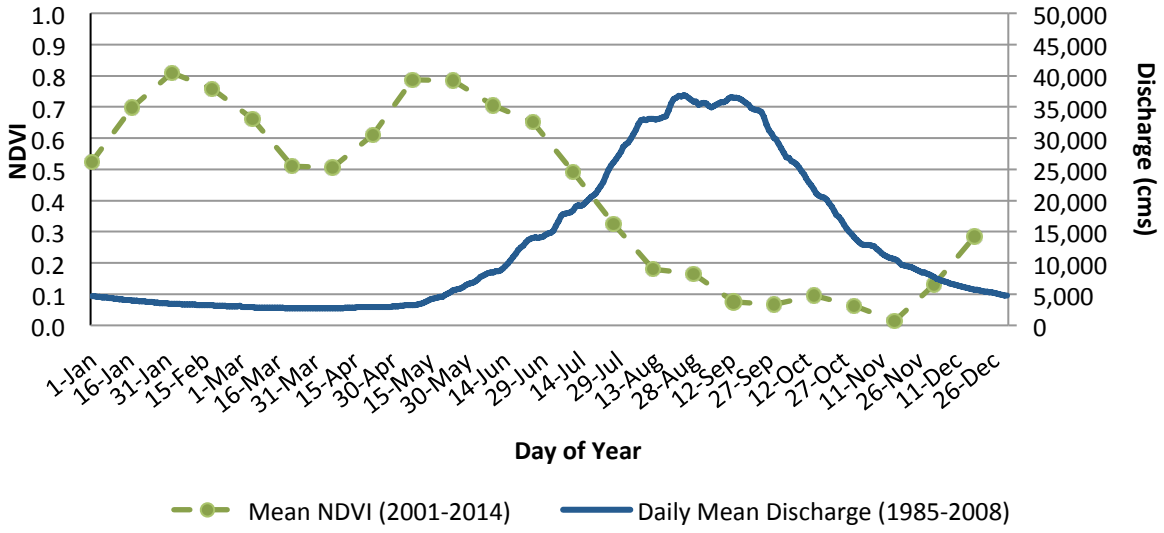

Figure 3.1: Time-series of Terra MODIS-derived NDVI from a rice paddy (green), mean daily river discharge (blue) from 1985-2008 of the Mekong River at Kratie, Cambodia. The effect of the seasonal flooding over the pixel is evident from the dynamic range of NDVI and river discharge climatology. The Mekong River Commission provided the river discharge data.

When using a change detection approach for flood mapping, choosing an appropriate reference baseline image is important to obtain accurate results (Hostache et al., 2012). Because of frequent cloud presence in the region, the dry season baseline needed to have cloud free coverage of the entire study area to be able to make any comparisons of NDVI. This study acquired temporally processed 32 day (i.e., monthly) composited 250m MODIS maximum NDVI products from the Forecast Mekong project (http://deltas.usgs.gov/fm/data/data_ndvi.aspx). These available NDVI composites were computed using a MATLAB-based Time Series Product Tool (TSPT) package in

conjunction with MODIS Aqua and Terra 8 day atmospherically corrected reflectance data (MYD09Q1 and MOD09Q1). The TSPT package was used to compute NDVIs from the reflectance data, applying MODIS QA data resident to each reflectance data set to eliminate poor quality data with atmospheric contamination and/or poor viewing geometry. The cleaned Aqua and Terra NDVIs were then fused with additional noise detection subsequently applied. Data void interpolation was then performed as needed, using NDVI values for dates before and after a given void within the time series at the pixel level, and then after void interpolation were re-aggregated into cloud free coverage of 32 day NDVIs across the entire study region for 2003-2011. A dry season baseline was then created by calculating the mean of the date 1 (January 1 – February 1) image from each year of 2003-2011. This baseline is meant to approximate the historical average NDVI during non-flooded conditions near peak greenness, as to maximize the potential difference in NDVI during flooded conditions, increasing likelihood of inundation detection.

For this study, the current NDVI was processed in a different manner from the historical baseline to accommodate production in a near real time environment. First, it was necessary to use MODIS multi-day composites to acquire a view of a flood event because of consistent cloud coverage in the region during the wet season. Various MODIS products are available to use for capturing flooding, including daily surface reflectance, 8-day surface reflectance, and 16-day vegetation indices from both Aqua and Terra satellites. In addition, the 32-day NDVI composites used to create the baseline could also be used for retrospective monthly flood assessment, which was useful for comparison to similar products generated using the near real time method. Using more days to compute the flood scene composite reduces cloud obstruction more effectively, but may do so at the expense of capturing the full flood progression. For many

applications, such as disaster relief and agricultural monitoring, a shorter viewing window of the flood may be more useful to capture the current situation. This study uses the MODIS 8 day surface reflectance products from both Aqua and Terra satellites (MYD09 and MOD09) for generating current NDVI images in order to demonstrate and assess the potential for a rapid assessment or near real-time flood detection product.

The MOD09Q1 8-day composite products provide atmospherically corrected surface reflectance data in the red (band 1, 620-670 nm) and near infrared (band 2, 841-876 nm) regions of the electromagnetic spectrum at 250 m resolution. Therefore, the following equation was used to calculate the NDVI from these bands at this spatial resolution for the date of interest containing a flood event.

$$NDVI = \frac{NIR\text{-}RED}{NIR+RED}$$

This 8-day product is produced for the same composite time for both Aqua and Terra MODIS separately (MYD09Q1 and MOD09Q1, respectively). The Aqua and Terra products were used to create an NDVI image from each sensor for the same 8-day period. Then, a maximum NDVI composite was produced from these two images to minimize atmospheric and cloud contamination, and produce the NDVI scene of the flood. This flood scene image was then used to compute the percent change in NDVI from the dry season baseline using the equation

$$\%\ Change\ NDVI = \frac{NDVI_{Flood} - NDVI_{Dry}}{NDVI_{Dry}} \times 100$$

Areas that experience a high percent decrease in NDVI represent areas that are more likely to be inundated or damaged by floodwater in the flood scene image.

Decreases on a given date of NDVI compared to the baseline can also be caused by other vegetation disturbances, topographic variability, and atmospheric contamination. Therefore, we performed several additional processing steps in order to reduce false flood detection in the final inundation product. The SWIR band from the MOD09A1/MYD09A1 products was also used to identify wet pixels, removing false flood detection due to other sources. SWIR wavelengths are highly sensitive to water content (Boschetti et al., 2014; Ji et al., 2009; Tucker, 1980; Xiao et al., 2002) and therefore clearly distinguish dry land from surface water. The SWIR band 6 of MOD09A1 and MYD09A1 products (1628-1652 nm) were composited and resampled to 250 m to match the percent change NDVI image. Any pixels that had a decrease in NDVI, but a high reflectance of SWIR were considered to not be flooded. In addition, the MODIS MOD44W water mask product was used to define permanent water bodies for reference.

Clouds are nearly entirely absent in the temporally processed historical 32-day products, but the current 8-day products still contain residual clouds that obstruct the view of flood extent. The cloud flags in QA information included in the MODIS products were used to detect and map clouds in the flood scene. The resulting inundation product shows the percent decrease in NDVI due to flooding, the permanent water bodies, and the residual clouds (Figure 3.2).

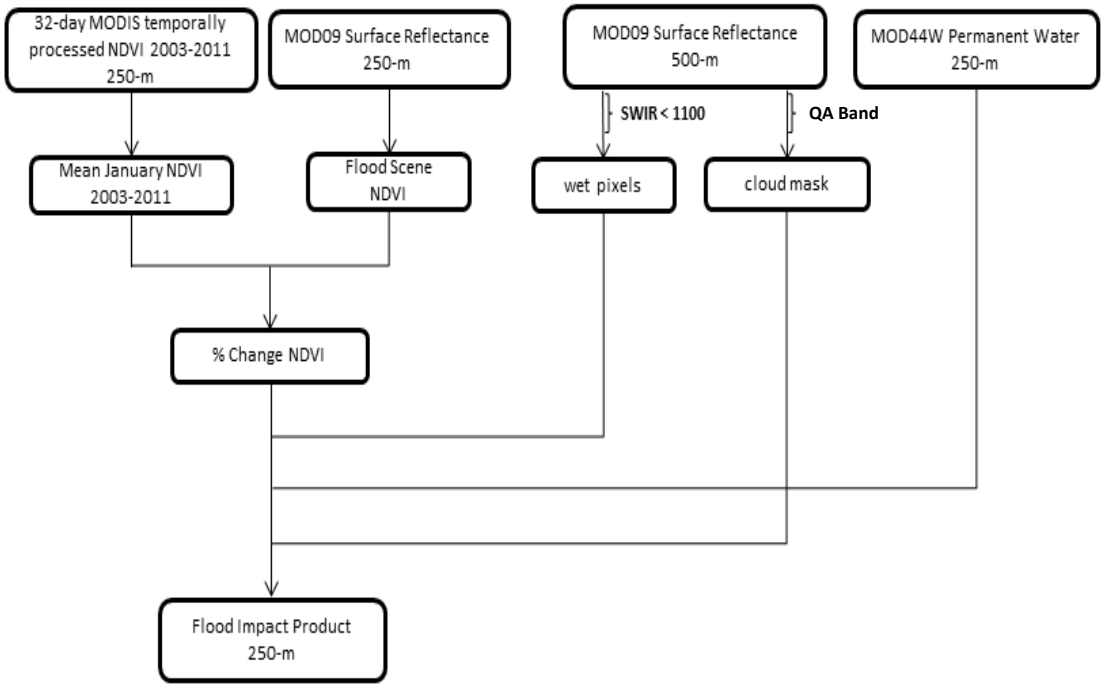

Figure 3.2: Data processing framework used to produce NDVI-based flood impact product from single-satellite MODIS flood scene image.

Validation

Although the resulting decreases in NDVI likely result from inundation, small decreases may be because of vegetation loss, wet but not flooded conditions, pixels with only a small portion inundated, or atmospheric changes such as cloud shadows. Therefore, we chose an empirically-derived threshold of a 30% decrease of NDVI or more to create a binary flood/not flood map for quantitative validation against radar maps and more qualitative assessment against higher resolution imagery, and to allow for small changes that may not be inundation.

First, the binary flood maps were compared to maps created from radar data during disaster events in 2011 and 2013. As radar data are known to accurately delineate surface water regardless of atmospheric conditions (Long 2001), these maps

were used as references for evaluating the accuracy of NDVI-derived flood extent. The 2011 flood event was one of the two worst floods, along with 2001, in recent history through much of the region. In response, the United Nations Institute for Training and Research (UNITAR) Operational Satellite Applications Programme (UNOSAT) created a flood extent map from ASAR data acquired on September 27 and 30, 2011. The 8-day MODIS composites for the overlapping period was too cloudy to make a quantitative comparison, so the MODIS product composite starting October 16, 2011 was compared against the UNOSAT map. The flood season of 2013, although not as spatially extensive, was estimated to cause more damage than the 2011 flood (MRC, 2015). The reference flood map for the 2013 season was a map created from COSMO-SkyMed and Radarsat-2 data acquired on October 8 and 9, 2013. This map was created by the European Commission's Copernicus Emergency Management Service (EMS) Mapping. The MODIS composite for the 2013 comparison begins on October 08, 2013, allowing for a more direct comparison against the EMS map. To assess the accuracy of the MODIS NDVI-based maps, we calculated the area of inundation in each of the 24 provinces of Cambodia for each MODIS and reference map, and we compared the areas with a linear regression and root mean square error statistics.

The utility of the inundation product was also evaluated by visually comparing areas of mapped flooding with higher resolution data from Landsat 5 TM, Landsat 7 ETM+, and the ISERV instrument on the International Space Station. Three dates over the 2006 wet season and one date during the 2013 flood season were validated against Landsat false color (using RGB 742) that clearly distinguishes water and land conditions, in order to assess product performance over the course of a calendar year. The year 2006 was a fairly typical flood year, including several tropical cyclones that caused extreme flood events in various parts of the basin, particularly later in the season (Mekong River

Commission (MRC), 2012). The region used for validation was the area surrounding the city of Phnom Penh, Cambodia, which is contained in Landsat WRS-2 path 126, row 52. We selected the dates for validation based on available Landsat scenes with sufficient cloud free coverage such that most of the flood event could be effectively viewed. Products for 2013 were chosen for evaluation, based on other available high-resolution imagery for additional analysis.

A random 300 pixels (150 flood, 150 not flood) were sampled from the flood extent map within the reference Landsat scene. Each randomly sampled 250-meter by 250-meter pixel was visually assessed against the Landsat RGB 742 false color image that accents water in blue and distinguishes water from vegetation and bare ground well. Areas that were cloudy in the reference Landsat image or intersected a scan line gap in the Landsat 7 data were excluded from the random sampling, as these areas could not be reliably assessed. Producer's accuracy, user's accuracy, overall accuracy, and kappa values were computed to determine the agreement of the MODIS NDVI product and the reference Landsat data for each of the dates. Although this validation method is subject to some interpretation error by the analyst, the expectation was that this approach would provide reasonably good estimates of the product performance and utility at the pixel level, both spatially and temporally.

For comparison with additional high-resolution data, I also validated the flood detection product for the 2013 date using the ISS SERVIR Environmental Research and Visualization System (ISERV), which collects true color image data from the International Space Station (ISS) (www.nasa.gov/mission_pages/station/research/experiments/867.html). The instrument was installed on the ISS in early 2013, with the first image captured on February 16, 2013. On November 1, 2013, ISERV captured images of a flood event in our study area,

just south of Phnom Penh, Cambodia. These images provide a unique opportunity to validate the product with multiple higher resolution datasets, since a Landsat 7 ETM+ image was acquired on the same day as the available ISERV imagery. The same method of validation was used with the ISERV imagery as with the Landsat reference data, but only 200 pixel samples were used because the area covered by the ISERV imagery was much smaller than that of the Landsat images.

RESULTS AND DISCUSSION

The flood maps derived from NDVI changes agreed well with the reference surface water maps, but with limitations primarily due to the use of an optical sensor. The MODIS NDVI derived flood extent map for the 2011 event agreed fairly well with the UNOSAT ASAR flood map at the provincial level, with a RMSE of 957.28 km^2 (n=24) and an R^2 value of 0.69 (Figure 3.3). In general, the MODIS map underestimated the flood extent, which is expected because the MODIS data were acquired two weeks after the ASAR data, when most gauge levels in the river were about a meter lower. But, the reason that date had to be used was because the prior two MODIS dates had too many clouds in the flooded area to make an accurate comparison. Persistent cloud cover during the rainy season poses the first limitation of the MODIS maps, which has been observed in other studies in the region (Fayne et al., 2017; Sakamoto et al., 2007). The provinces with the biggest difference in flood area detected were Banteay Meanchey and Battambang, to the northwest of Tonle Sap Lake (Figure 3.3). Flooding in this area is known to be difficult to detect with optical sensors such as MODIS due to the high green canopy of the forests to the northwest of Tonle Sap Lake (Sakamoto et al., 2007). Although most of the floodplain is agriculture and short vegetation, detecting flooding under the forest canopy around Tonle Sap Lake remains another limitation when using

MODIS, or any optical sensor. When comparing the maps in all of the provinces except for Banteay Meanchey and Battambang, however, the RMSE is 565.94 km^2 (n=22) and an R^2 value of 0.94. The higher R^2 correlation but with the moderate RMSE suggests that the disagreement could likely be due to the difference in dates of the data used for each map, the resolution difference, or the threshold value chosen for the extent map derived from MODIS NDVI changes.

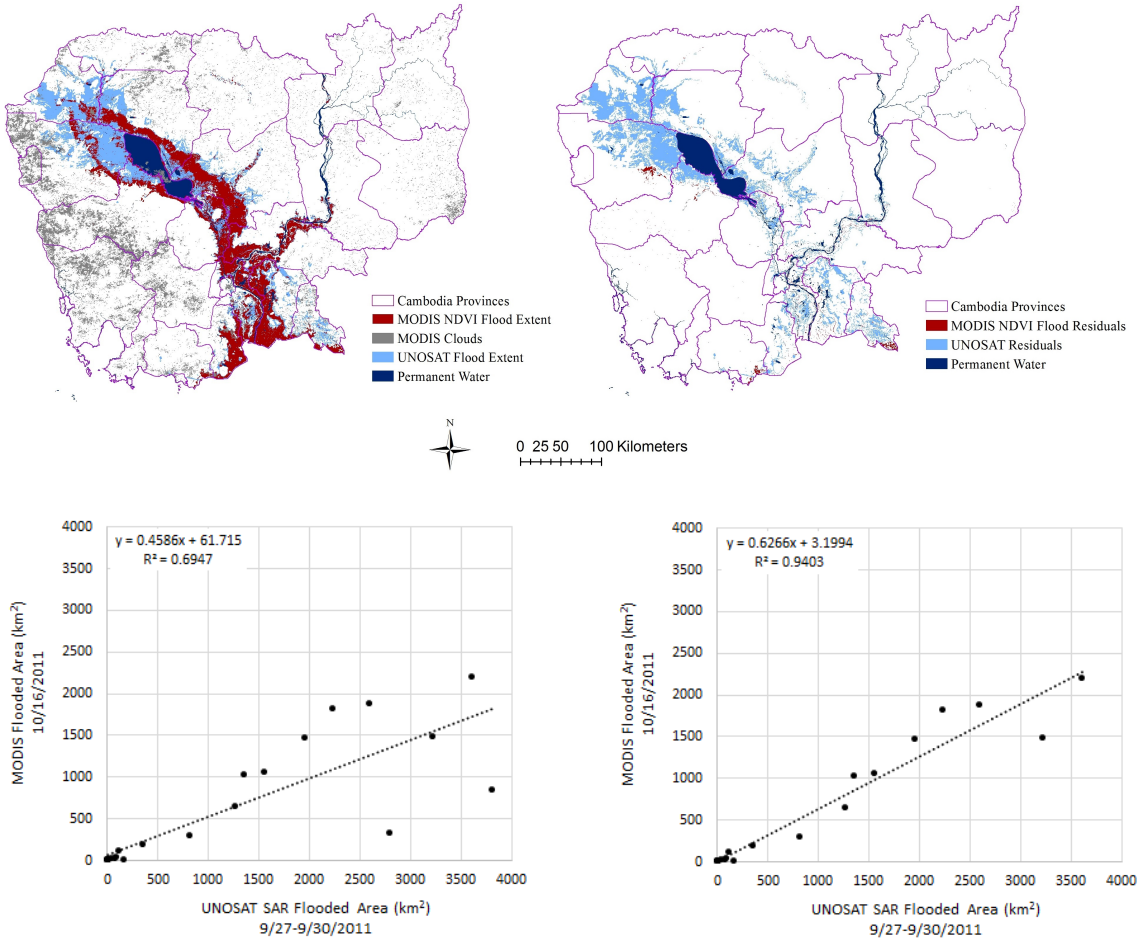

Figure 3.3: Comparison of MODIS derived flood map with SAR map for October 2011 event.

The 2013 MODIS flood extent map agreed more closely with the reference map from COSMO-SkyMed and Radarsat-2 data than the 2011 comparison. Including all provinces, the 2013 comparison resulted in an RMSE of 239.29 km^2 and an R^2 value of 0.87 (n=24)(Figure 3.4) For this October 8, 2013 comparison, the largest source of difference was due to clouds over part of the flood in the southern provinces Prey Veng and Takeo. In most provinces not affected by clouds, the MODIS NDVI product actually estimated slightly more flood than the Copernicus EMS map. When comparing all of the provinces except the Prey Veng and Takeo, the RMSE is 152.07 km^2 and the R^2 value is 0.95 (n=22) (Figure 3.4). The close agreement of the MODIS NDVI flood extent with the 2011 and 2013 radar maps suggests that the relative decreases in NDVI, and the threshold of 30% decrease, correlate closely with flood inundation.

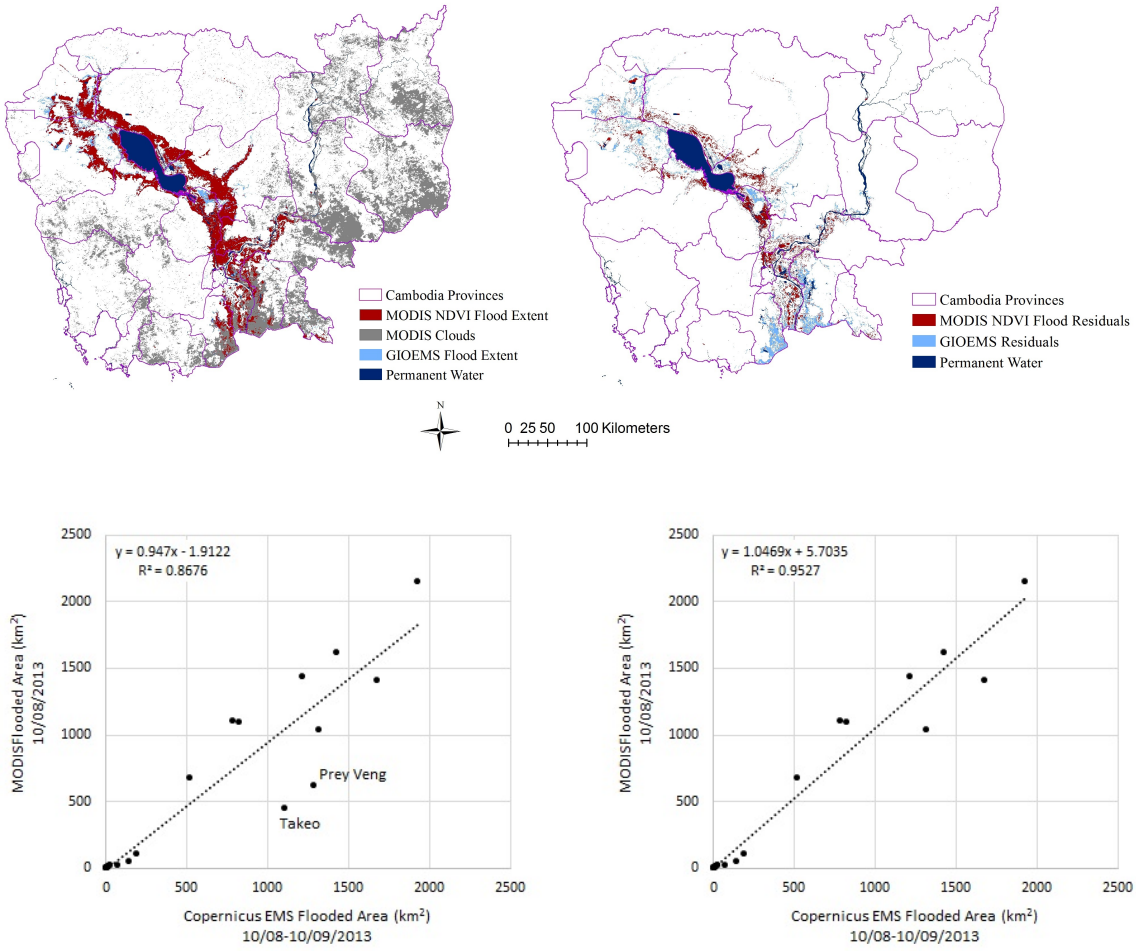

Figure 3.4: Comparison of MODIS derived flood map with SAR map for October 2013 event.

The NDVI-based flood impact products reveal inundated areas and demonstrate utility for rapid flood assessment and monitoring (Figure 3.5). The NDVI change products agreed well with image analyst interpretation of random locations on Landsat false color (RGB 742) images for the 3 dates in 2006 (Figure 3.5; Table 3.1). Consistently high overall agreements of 92.33%, 94.67%, and 93.00% for the September, October, and November 2006 dates, respectively, suggest very high utility of this inundation product for continuous flood assessment throughout the season (Table 3.1;

Figure 3.5). All three dates showed very low omission errors (1-Producer's Agreement) for the flood class (0.050, 0.053, and 0.043) suggesting that the product rarely omitted flooded areas. The low commission errors (1-User's Agreement) yielded values of 0.107, 0.533, and 0.100, suggesting that this method does not substantially over-classify flooded areas, although it is more likely to over-classify than it is to omit flooded pixels.

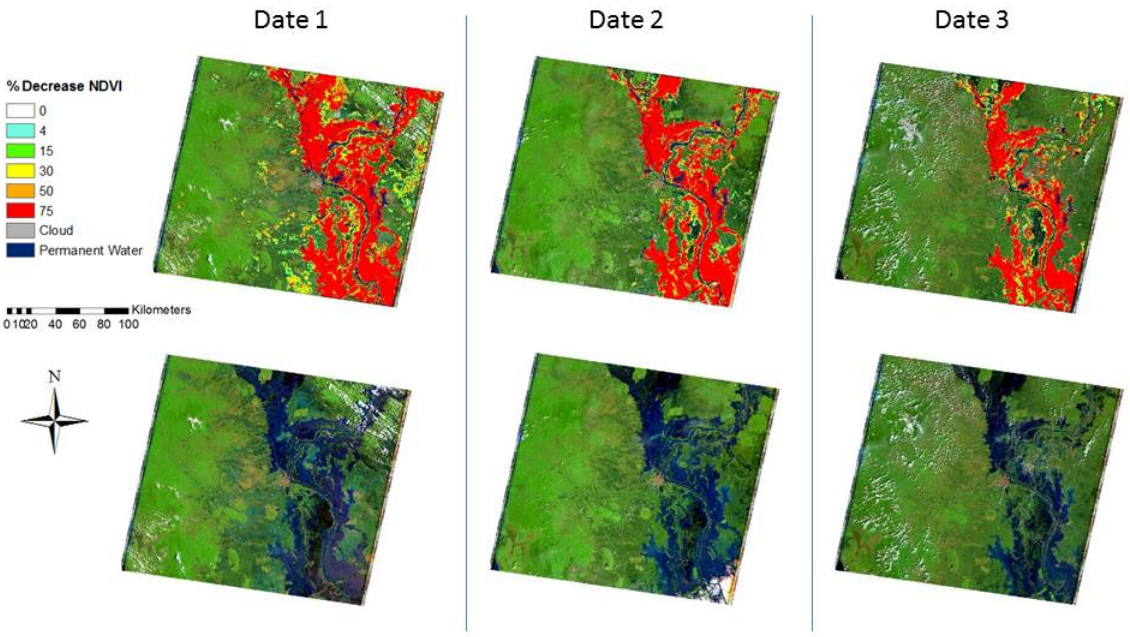

Figure 3.5. Landsat scenes (bottom) used for validation of the corresponding MODIS NDVI change product (top) of the region surrounding Phnom Penh, Cambodia. Landsat scenes (Path/Row 126/52) are displayed in false color RGB 742. (Date 1) MODIS NDVI change product from 8 day composite acquired 8/29 – 9/5/2006; Landsat 5 TM acquired 9/3/2006. (Date 2) MODIS NDVI change product from 8 day composite acquired 10/16 – 10/23/2006; Landsat 5 TM acquired 10/21/2006. (Date 3) MODIS NDVI change product from 8 day composite acquired 11/1 – 11/8/2006; Landsat 5 TM acquired 11/6/2006.

Table 3.1: Agreement of MODIS NDVI change flood detection product compared to Landsat RGB 742 (P/R: 126/52) displays during the 2006 flood season.

Validation Date	MODIS Composite	Reference Data	Class	Producer's Agreement	User's Agreement	Overall Agreement	Kappa
Date 1	8/29 - 9/5/2006	Landsat 5 9/3/2006	Flood	95.00%	89.33%	92.33% (277/300)	0.8467
			Not Flood	89.90%	95.33%		
Date 2	10/16 - 10/23/2006	Landsat 5 10/21/2006	Flood	94.67%	94.67%	94.67% (284/300)	0.8933
			Not Flood	94.67%	94.67%		
Date 3	11/1- 11/8/2006	Landsat 5 11/6/2006	Flood	95.74%	90.00%	93.00% (279/300)	0.8600
			Not Flood	90.57%	96.00%		

Table 3.2: Agreement of MODIS NDVI change flood detection product compared to Landsat RGB 742 and ISERV true color imagery during the 2013 flood season.

Validation Date	MODIS Composite	Reference Data	Class	Producer's Agreement	User's Agreement	Overall Agreement	Kappa
Date 4	11/1 - 11/8/2013	Landsat 7 11/1/2013	Flood	94.00%	94.00%	94.00% (282/300)	0.8800
			Not Flood	94.00%	94.00%		
Date 4	11/1 - 11/8/2013	ISERV 11/1/2013	Flood	82.91%	97.00%	88.50% (177/200)	0.7700
			Not Flood	96.39%	80.00%		

The tested flood detection products also performed very well when compared to image analyst interpretation of random locations on high resolution ISERV imagery from November 1, 2013, yielding a high overall agreement of 88.50% (Table 3.2). In addition, a comparison with Landsat imagery also from November 1, 2013 resulted in an overall accuracy of 94.00% (Table 3.2). When compared to the ISERV imagery, the flood class produced a higher omission error rate than when compared to Landsat 7 data of the same date (0.171 vs. 0.06) or any of the other Landsat comparisons. The higher omission error when compared to the ISERV imagery could be due to the higher resolution of the

reference data, showing the edges of the flood and areas that have been inundated that still have some vegetation, that are not picked up by the 250 m resolution data sets. It may also be that the Landsat false color imagery shows land versus water (especially turbid water) more clearly compared to the ISERV imagery. In addition, it is possible to distinguish algae and green vegetation on the surface of the water in the Landsat and ISERV imagery. Aquatic vegetation may increase the NDVI value of the pixel, which can reduce the relative decrease caused by the flood water to below the threshold for what was classified as flood, omitting these pixels from the thresholded flood extent product (Figure 3.6). It is conceivable that a more conservative NDVI change threshold could improve results, but more research and field data are needed to confirm. The overall high agreements of the flood product assessment against both ISERV and Landsat imagery, however, support both the utility of the product for inundation detection, as well as the validation technique using various reference data.

Both the Landsat false colors and ISERV imagery proved useful for validation of the MODIS-based inundation product (Figure 3.6). The many spectral bands of Landsat data allows for false color viewing of wavelengths that clearly distinguish between water and land. In addition, the 30 m false color Landsat pixels are high enough resolution to distinguish mixed pixels of the 250 m NDVI change product, but still cannot distinguish water features smaller than 30 m. The ISERV imagery has a higher spatial resolution, but it is limited to natural color, and has a more limited availability and spatial extent. The turbidity of the floodwater can make it difficult to distinguish water from bare ground in some areas found on these natural color images (Figure 3.6). As result, the false color Landsat data were used to confirm the distinction of bare ground and turbid water during validation of the product. Large algal mats and high canopies can also make interpretating what is flooded underneath this vegetation difficult with any space borne

optical imagery. Lastly, frequent cloud coverage in the region during the rainy season reduces the number of useable images that are taken by either Landsat or ISERV. These characteristics render these data sources less practical for continuous and timely inundation monitoring, but allow them to be very useful for validating coarser resolution products, especially when used together. Although the visual assessment against higher resolution is subject to human error by the analyst, it still allowed for a pixel level comparison for general agreement. Additionally, the analysis allowed for a qualitative investigation of the effect of mixed pixels and shallow flooding on the degree of decrease in NDVI.

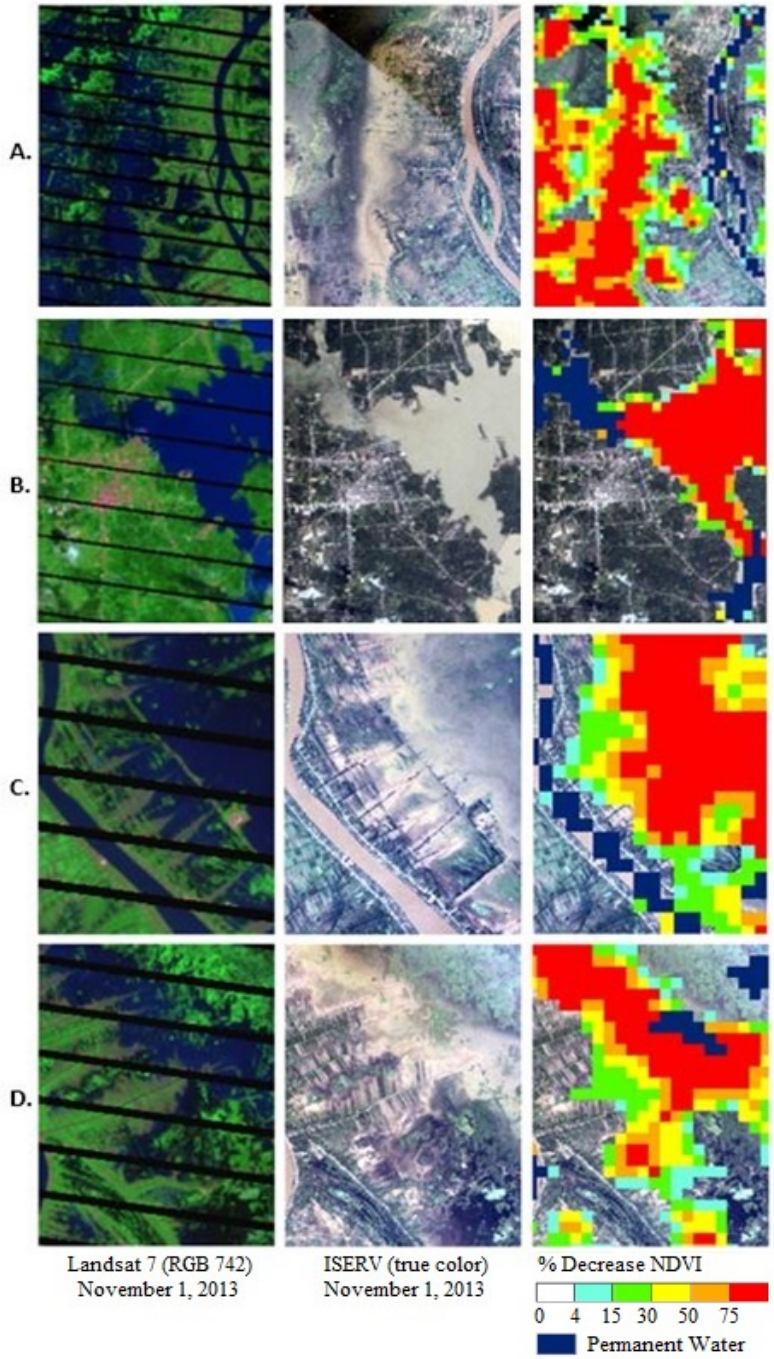

Figure 3.6: Comparison of inundation product from 8-day composite starting 11/1/2013 (right; overlain on ISERV) with ISERV natural color imagery (middle) and Landsat 7 ETM+ false color (RGB 742; left) from 11/1/2013 demonstrates degree of flooding and partially flooded pixels represented by the amount of decrease in NDVI.

When comparing the MODIS flood detection product to either the ISERV or Landsat imagery, the percent decrease in NDVI consistently shows a visual correspondence in terms of flooded versus non-flooded areas (Figure 3.6). For example, the warmer colors, corresponding to more drastic decreases in NDVI, consistently show fully inundated areas. The cooler colors, representing less decrease in NDVI, correspond with the edges of the flood as the inundation becomes shallower, so that vegetation is still visible under the water, and mixed pixels that have both flood and dry land or vegetation in them (Figure 3.6). Because NDVI is affected by vegetation and saturated soil bottom characteristics of rice paddies (Boschetti et al., 2014), this NDVI change approach can be utilized in this region for determining relative difference in inundation severity. Visualizing the decreases in NDVI as corresponding to the degree of flood allows for an intuitive interpretation of the distribution of floodwater and likelihood of damage, particularly in agricultural areas, although is limited for deriving quantitative depth. The flood detection method evaluated in this study showed high potential for providing timely valuable insight in the location and extent of flooding in the LMB across the calendar year, which could be useful for aiding disaster, agricultural, and water management in the region.

CONCLUSIONS

This study demonstrated a novel approach for mapping flood impact zones in the Southeast Asia region. In doing so, wet season anomalies of NDVI values were detected within flood prone low-lying areas to assess relative impact. The MODIS sensors on board the Aqua and Terra satellites provide data at a high enough spectral, spatial, and temporal resolution to detect disturbances in the land surface that are due to flooding with

high enough accuracy for practical applications. The MOD09 and MYD09 8-day MODIS surface reflectance products were successfully used in this study to map flood inundation in the LMB at 250 m resolution, despite persistent cloud coverage in the region. The results for 2006 and 2013 showed high agreement with available higher resolution reference satellite data, with greater than 90% agreement for the Landsat comparisons, and 88% agreement when compared to ISERV imagery. The validation process also demonstrated a practical application of the ISERV instrument on board the ISS. Not only can this instrument provide imagery during a disaster, but can also provide high-resolution reference data for validating other types of disaster-related products. The qualitative comparison with higher resolution data also suggests the degree of decrease in NDVI reflects the relative degree of flooding, although not quantitative depth. This methodology, therefore, can be used to assess the degree of flood impacts and the distribution and severity of inundation across the LMB, particularly useful for disaster relief and agricultural monitoring.

The flood detection methodology from this project can be used for assessing historical flooding in the region. This consistent data collection and relatively simple streamlined methodology suggests that the process can also be automated for near real-time continuous flood monitoring throughout the monsoon season, or deployed immediately following a disaster. Since MODIS data are collected continuously, there is no need for satellite tasking and the entire region can be continuously monitored at the same time. Having medium-resolution inundation impact maps in a timely manner can provide disaster relief and management teams with up-to-date information on where response is needed the most. Additionally, these products can be used to assess the greatest extent of flooding and lasting damage after the event to help determine the appropriate allocation of recovery resources and efforts to the areas that need it most.

The NDVI-based methodology for detecting seasonal flooding developed by this study for the LMB may also be implemented and adapted for observing other flood assessment information. The method may not be as effective for flood prone areas without distinct dry and rainy seasons. Other methods may work better in other regions. For example, NDVI change based on comparison a given current 8 day NDVI to a mean NDVI for the same 8 day interval may work better in temperate regions that are infrequently and irregularly flooded.

The methodology demonstrated in this study has significant potential for use in near real-time inundation monitoring. Daily MODIS surface reflectance products could be acquired from the NASA Land, Atmosphere Near Real-time Capability for EOS (LANCE) server, where they are stored within 3 hours of acquisition. Because frequent cloud cover is a common issue during the monsoon season, compositing of multiple daily Aqua and Terra MODIS images may be required to derive wall to wall cloud free current looks. Lastly, other optical sensors may be utilized using the same method, increasing the timeliness and potential resolution of inundation detection. For example, the Visible Infrared Imager Radiometer Suite (VIIRS), Landsat, and Sentinel-2 sensors all contain data in the red and NIR regions of the electromagnetic spectrum, which allows for the calculation of NDVI. Eventually, VIIRS will need to be used as a follow-on to the MODIS sensors once they are decommissioned. Data integration techniques could be applied to utilize as many platforms as possible for the mostly timely and synoptic detection of floods using the NDVI-based approach. Future work should also explore implementing this technique in other regions where an appropriate dry season baseline is needed for improving flood mapping. Employing this method in a near real-time system to detect flood impacts and abnormal flood conditions could greatly assistant regional

disaster, agriculture, and water management decision makers for year-round flood assessment.

Chapter 4: Detecting Rice Agriculture at Risk to Extreme Flood and Drought Conditions

INTRODUCTION

Extensive rice agriculture in the floodplain of the Mekong River supports the well-being and economy of the region (Mekong River Commission (MRC), 2011) (Figure 4.1). In fact, the LMB supports over 10 million hectares of rice agriculture alone (ICEM, 2013). Although some of this agriculture is irrigated, much of it depends on the annual flood pulse of the river. As such, changes in the timing or intensity of annual flooding can have devastating effects on food production. Intensified floods and droughts caused nearly 90% of rice production losses in Cambodia during 1996-2001 (MRC, 2009). As shown in Chapter 2, there does not seem to be a directional trend in flood magnitude or timing, but land use change and hydropower development may be making the timing and magnitude of flooding less predictable. Increased flood season variability makes it difficult to properly plan planting and harvesting schedules. Estimating damage to agriculture from droughts and floods from the ground can be very difficult and time consuming. Satellite remote sensing, on the other hand, can provide comprehensive coverage both during and after the disaster. Comparing current conditions of flood and drought with historic trends and conditions can help provide immediate information on the relative degree of the situation and likelihood of damage. Here, I propose the use of comparing flood and drought situation satellite data with historic trends and statistics to reveal agricultural areas that are abnormally wet or dry. By doing so, we can estimate the location and extent of potential agricultural damage during the growing season and immediately following an event.

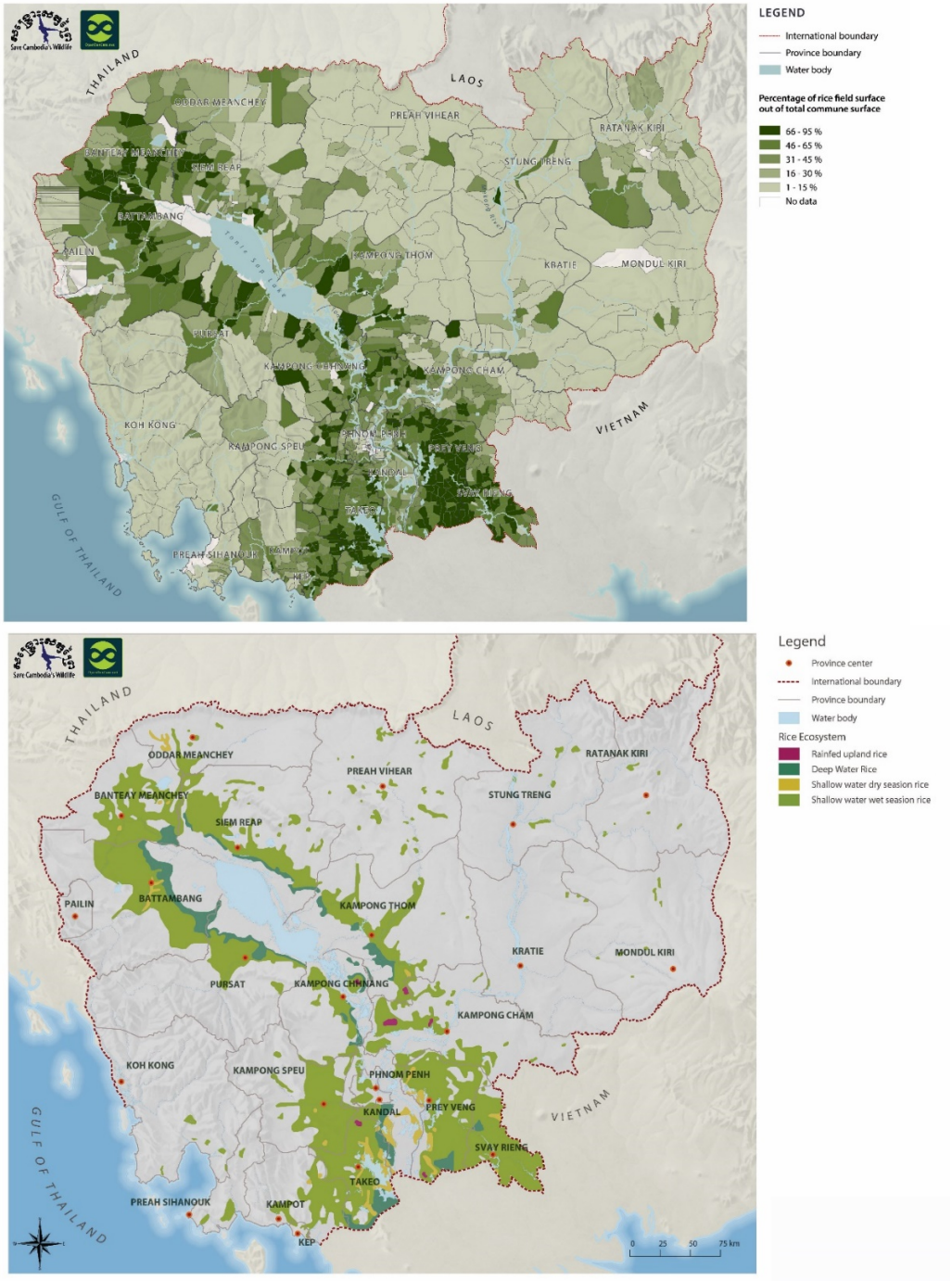

Figure 4.1. Location of areas suitable for different rice cultivation strategies (top) and percent of communes that are covered by rice paddies (bottom) in Cambodia.

Detecting flood and drought damage

Vegetation generally has a positive NDVI value, with healthier vegetation being close to 1. Although bare ground and concrete have very low NDVI values, water has the lowest values, which are generally negative (Figure 4.2) (Fayne et al., 2017). As such, rice paddies have a positive NDVI value through the dry season, but drop drastically when inundated during the wet season (Figure 3.1). As shown in the previous section, comparing seasonal changes in NDVI can be used to detect current flood extent. In this study, I compare MODIS 16-day NDVI values during the wet season to historical conditions during the same time of year to reveal areas that are at risk of extreme flood or drought. Because the people in this region rely upon and are adapted to the regular seasonal flooding, the mean NDVI value for 2005 – 2014 were used to represent the historical average flood conditions that people are adapted to and expect.

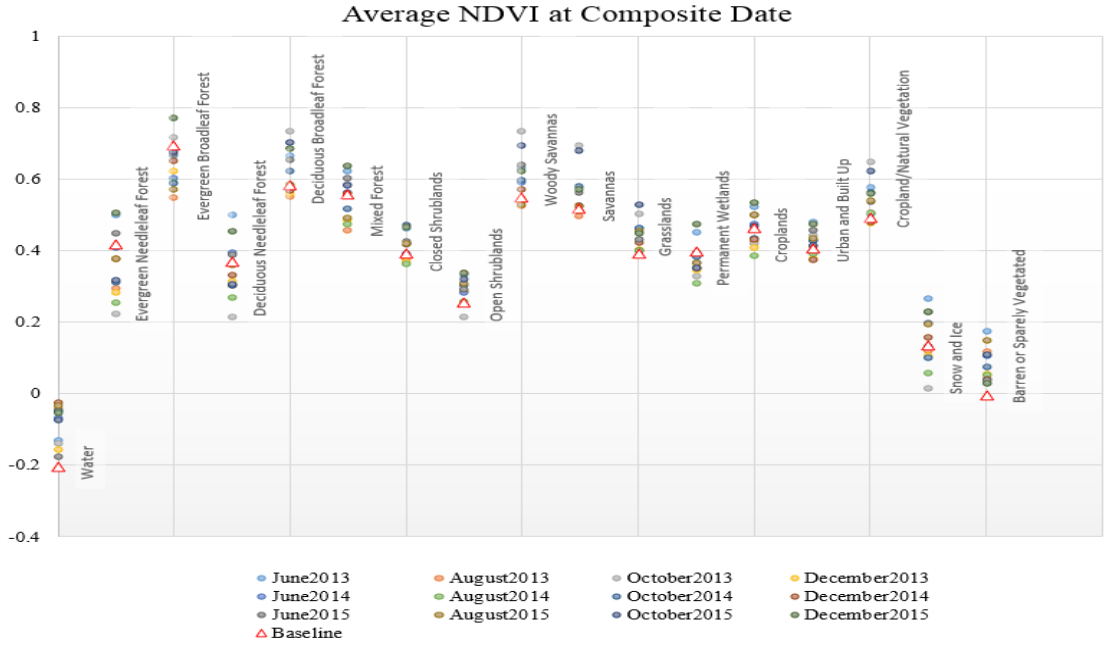

Figure 4.2: Average NDVI values from MODIS 250-m data for different land cover types defined by MODIS Land Cover Classification product (MCD12Q1) (From Fayne et al. 2017).

METHODOLOGY

The 2011 flood season was one of the two worst floods in the last 50 years, along with 2000, as measured at the three gauge stations (Figure 4.3). The 2015 season on the other hand, is one of the worst droughts in regional history. The gauges more downstream have less sporadic, smoother, hydrographs because these locations have a much larger floodplain and so they have less flashiness than the Kratie gauge (Figure 4.3). In all three hydrographs, the gauge height on October 16, 2011 was several meters higher than the historical average, and several meters lower than the average during 2015. Therefore, these two events, the 2011 flood and 2015 drought, were selected for testing the proposed methods.

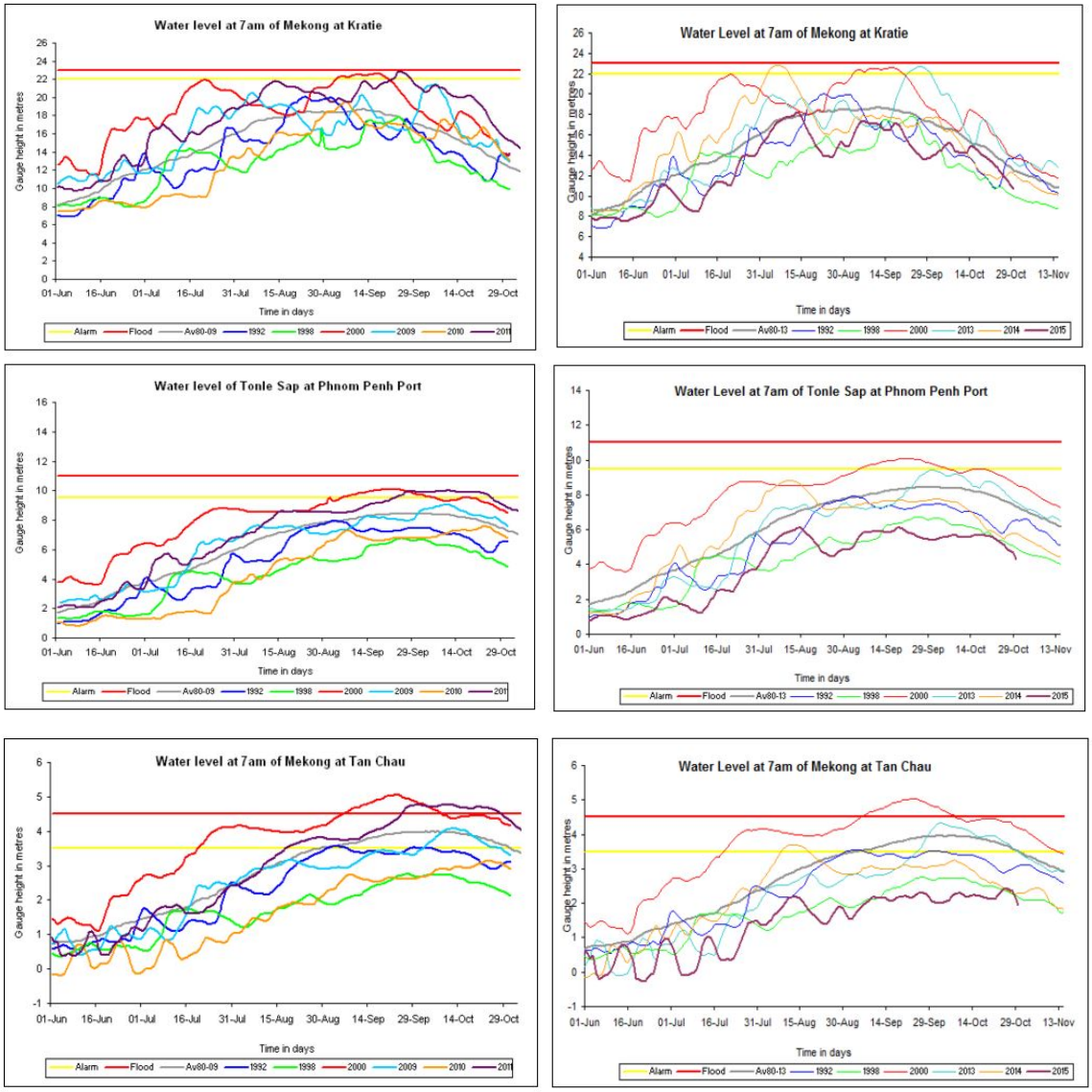

Figure 4.3: Wet season hydrographs of Mekong River at Kratie, Phnom Penh, and Tan Chau in Cambodia. 2011 flood and other events on the left, and the 2015 drought shown on the right. Graphs acquired from Mekong River Commission.

I calculated the mean and standard deviation NDVI were for the 16-day MODIS composite beginning October 16, for the years 2005-2014. I chose this date because the data were relatively cloud free during the extreme flood event of interest (2011), and is

consistently under flood conditions but after peak flooding occurs. The NDVI values from October 16, 2011, one of the worst floods in recent history, were compared to the historical statistics to reveal areas that are not normally flooded during the last decade, but were inundated during this event. Values that are *below* two standard deviations from the mean are interpreted as pixels that are flooded that are not normally during this time of year, and therefore at risk to damage. The reason for this is because the extremely low NDVI value of the water will be significantly lower than under non-flooded conditions. Values below one standard deviation are interpreted as areas at risk, but not as severe as those below two standard deviations.

The NDVI values from October 16, 2015, one of the worst droughts in history, were compared to the historical statistics to reveal areas that are normally flooded, but were not inundated during the drought. The values of these areas will be higher than they would be under flooded conditions. Therefore, pixels with NDVI values *above* two standard deviations of the historical mean are interpreted as being at risk to drought because they are not receiving the floodwater they normally get and depend upon. Values above one standard deviation are also at risk to drought damage, but not as severe as above two standard deviations.

RESULTS AND DISCUSSION

The mean NDVI for 2005 – 2014 shows that the flooding generally has a very low NDVI value compared to the rest of the region (Figure 4.4). In addition, the flooded areas tend to have more variability in NDVI values from year to year than the rest of the region, except for the mountainous regions. This trend is due to the variation in flood

extent and height from year to year in the floodplain, and the susceptibility of the data to be obstructed by terrain shadows in the mountainous areas.

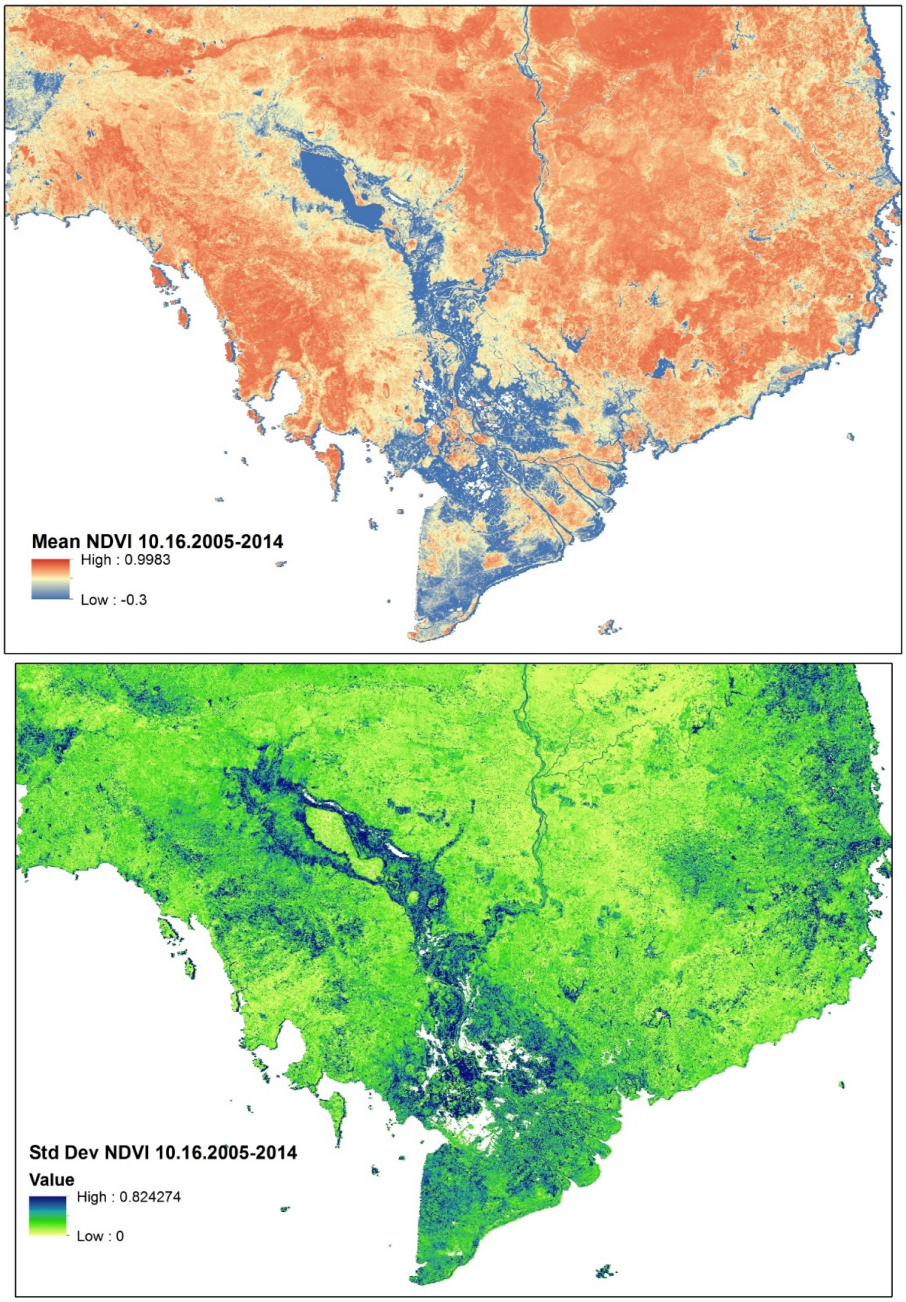

Figure 4.4. Mean NDVI (top) and standard deviation of NDVI (bottom) of the study area on October 16 for the years 2005-2014.

In the 2011 flood, pixels that have NDVI values below two standard deviations of the historical mean reveal abnormal inundation that could be damaging to the rice production. The results show these areas occur around the edges of the flood extent where the abnormal extent would occur (Figure 4.5). This observation suggests that this method of comparing NDVI to historical statistics for that same period of time does reveal abnormal flooding of areas that are not normally inundated. In order to confirm whether these rice paddies are actually damaged by the end of the season, however, more information and detailed investigation is necessary. One approach could be to use higher resolution data during the harvest period to assess the outcome of the rice crop. White areas in Figure 4.5 are areas that were omitted by the QA band, although they are clearly areas of inundation and not cloud. Further investigation is needed to assess how the QA band is determining low quality pixels to include these areas in the calculations.

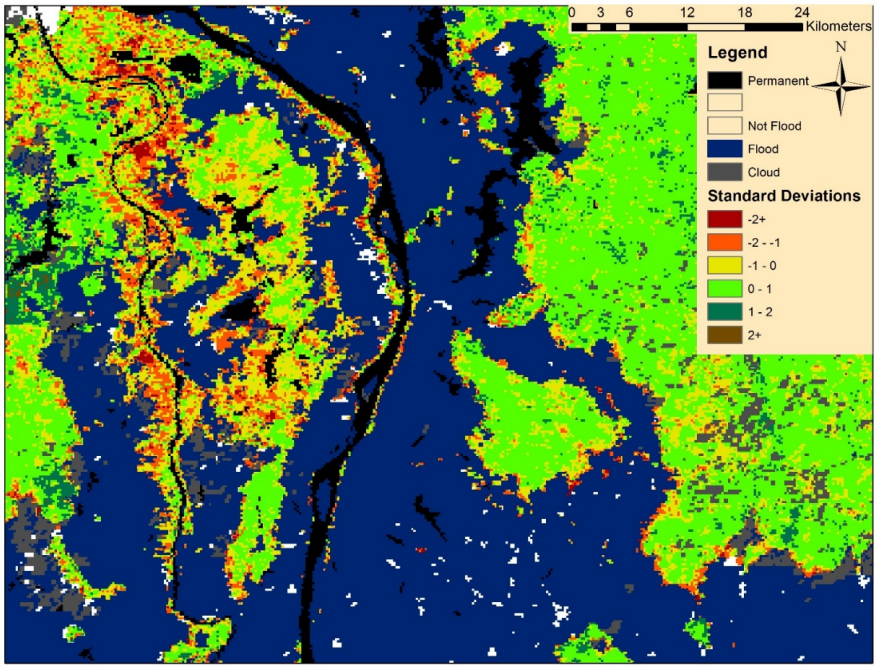

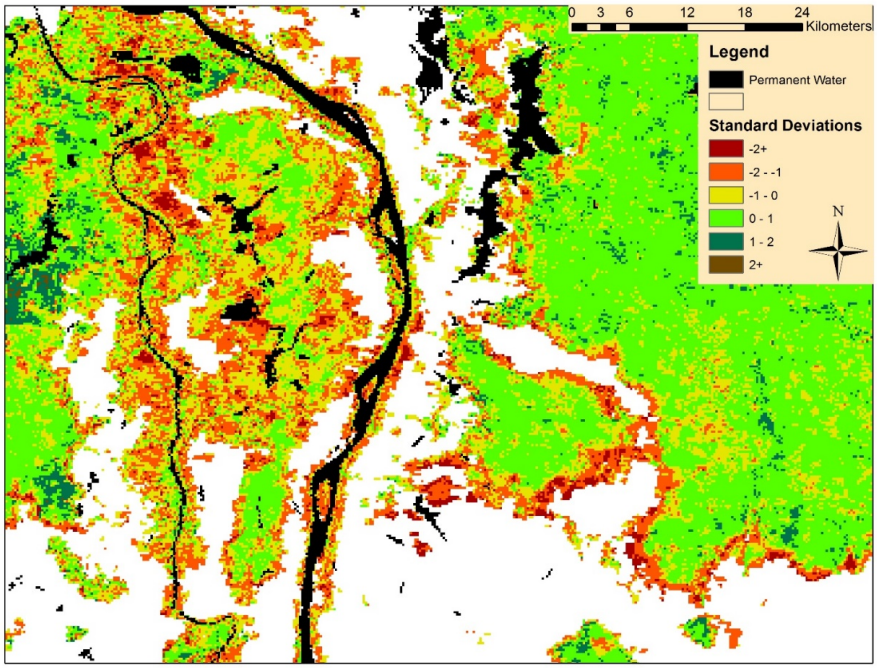

Figure 4.5. Flood extent on October 16, 2011 overlain on the standard score for that date compared to average conditions for this period for the years 2005-2014 (top) and the z-score for 10/16/2011 compared to the historical statistics (bottom).

In the 2015 drought, pixels that have NDVI values above two standard deviations of the historical mean reveal abnormal dryness that could be damaging to the rice production. The results show these areas occur in areas in the flood plain that are generally flooded most years but are dry during this event (Figure 4.6). This observation suggests that this method of comparing NDVI to historical statistics for that same period of time does reveal drought-affected areas that are normally inundated. These areas in rice paddies are likely to be lost, as the fields are not receiving the necessary water that they normally receive from the annual flood pulse. Additionally, areas that have NDVI values more than two standard deviations below the mean could either be areas that are flooded that are not normally, as with the 2011 flood, or pixels that are not normally flooded but experiencing vegetation damage due to the drought. In order to confirm whether these rice paddies are actually damaged by the end of the season, however, more information and detailed investigation is necessary. One approach could be to use higher

resolution data during the harvest period to assess the outcome of the rice crop, as well as evaluating the actual value of NDVI through the rest of the growing season. White areas in Figure 4.6 are areas that were omitted by the QA band, although they are clearly areas of inundation and not cloud. Further investigation is needed to assess how the QA band is determining low quality pixels to include these areas in the calculations.

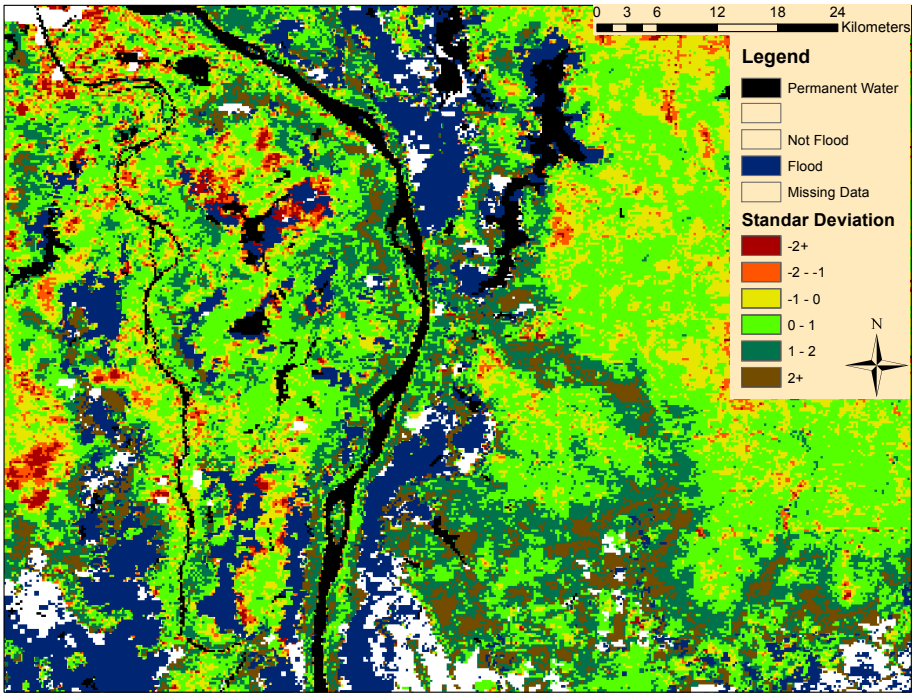

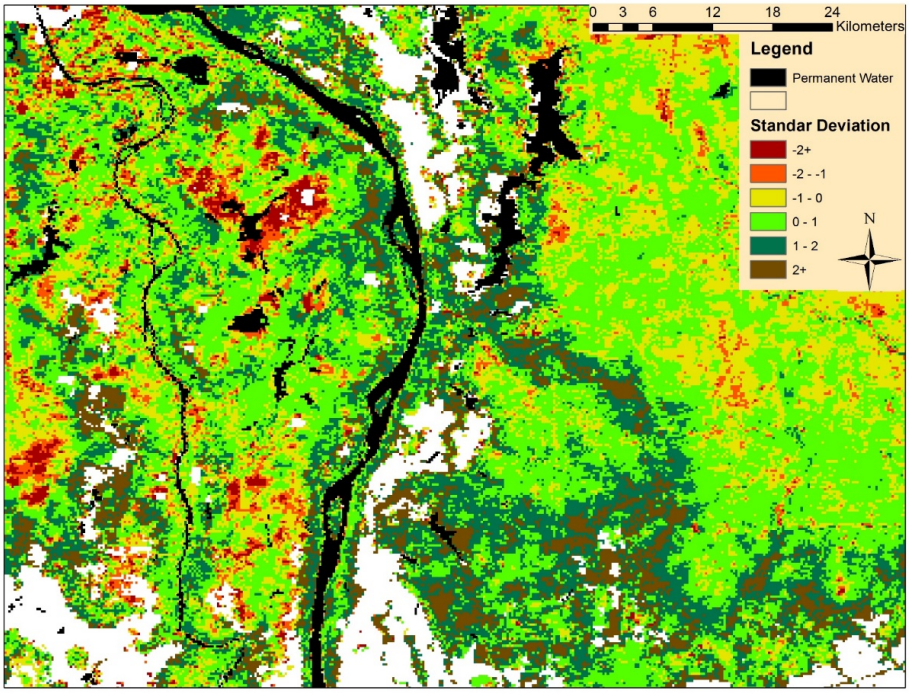

Figure 4.6: Flood extent on October 16, 2015 overlain on the standard score for that date compared to average conditions for this period for the years 2005-2014 (top) and the z-score for 10/16/2011 compared to the historical statistics (bottom).

CONCLUSIONS

The Lower Mekong Basin is a region that is particularly susceptible to changes in river hydrology due to climate change, population growth, and hydropower development. All of these factors have contributed to the occurrence of both abnormally devastating floods and droughts in recent years. As this region produces a significant portion of the world's rice production and local fish production that both depend upon the regularity of the annual flooding of the Mekong River, damage to these industries threatens the well-being of the millions of residents of the LMB. The annual flooding replenishes the soil and maintains fertility in the floodplain that is ideal for growing rice. Additionally, the annual flooding provides natural irrigation for the rice crops, which allow for 2, and even up to 3 crops a year. Since the rice crops are planted in coordination with the seasonal

flood pulse, a change in the timing or length of the flood season can damage the fields and reduce yields. Additionally, the increase in extreme flood and drought events have also threatened rice production, including the current droughts that are thought to be the worst in history. Although *in-situ* stream gauge data can tell us how the flood height and timing of the flood season is changing in historical context, it cannot be used to assess the spatial distribution of flooding. Remote sensing technology, however, provides temporally dense data across the entire region that can be used to monitor and assess floods and droughts in near real-time.

Analysis of peak discharges as measure data at Kratie, Cambodia, the benchmark for the system, reveals that changes in the flood pattern that could be detrimental to rice production. Although there is no linear trend in changes in the start and end of the flood season, it appears that the timing of the start and length of the flood season is becoming more variable. More investigation would allow more confident conclusions. If the flood season is starting at less consistent times, and the length of inundation of the paddies is less consistent, it is more likely that these fields will receive too much or not enough water at the incorrect time in the cropping cycle, putting these fields at risk of damage. Remote sensing offers the potential to monitor these changes in the annual floods and predict areas that are likely to be damaged by extreme flood or drought.

MODIS NDVI 16-day composite data provide information on how flood or drought conditions compare to historical averages to reveal flood-irrigated agriculture that is at risk. Comparing the current NDVI values to the mean of the last 10 years can be used to detect anomalies in rice paddy conditions. The analysis of the 2011 flood shows that the areas that have NDVI values below one standard deviation of the historical mean are the areas that are flooded but are not normally during average conditions, with an increasing z-score corresponding to increasing risk. In an extreme flood event, this could

drown crops that are not used to being inundated during that time in their phenology. The analysis of the 2015 drought demonstrates that comparing the NDVI to the historical mean of that same time of year reveals rice paddies that are normally inundated during this time of year, but are instead dry. These areas are likely to be damaged from drought conditions. Abnormally low NDVI values during this time would correspond to either areas that are flooded but not normally, or more likely also abnormally dry and suffering from drought, either way representing abnormal conditions. Taking into account the actual NDVI value, as well as the water-sensitive NIR wavelengths, could reveal these area's condition.

With severe droughts persisting throughout the region, it is crucial that transboundary drought and flood monitoring can be comprehensive enough to mitigate potential damage. This study demonstrates the use of MODIS NDVI data to reveal the spatial distribution of anomalous flood and drought conditions that can damage flood-irrigated rice agriculture. Although more validation is needed to make quantitative assessments, the methods proposed here show potential for monitoring and predicting damage to rice agriculture in near real-time in the LMB. Using this approach can provide information of at-risk crops during a flood or drought event allowing for preventive measures to be taken and minimize damage.

Chapter 5: GIS and Remote Sensing for Rapid Socio-economic Impact Assessment

INTRODUCTION

Globally, floods cause more economic, social, and humanitarian damage than any other type of natural disaster (UNISDR, 2015). In the Lower Mekong River Basin, flood disasters, such as those in 2011 and 2013, have resulted in millions of dollars of damage, directly affected millions of people, and claimed many lives (ACAPS, 2011; ADB, 2014; International Federation of Red Cross and Red Crescent Disaster Relief Emergency Fund, 2011; MRC, 2015). As the river flows through six countries, coordinating disaster management and relief efforts is a transboundary issue. As these floods occur on such a large scale, having up-to-date information on flood extent and damage estimates is essential for effective disaster relief and management efforts. Estimating the extent and impacts, such as affected population, of such large floods from the ground, however, is extremely difficult and impractical. As demonstrated in previous chapters, remote sensing provides an invaluable resource for monitoring flood extent and conditions across the entire Lower Mekong River Basin. By combining satellite-derived flood maps with socio-economic data in a Geographic Information System (GIS) can provide information on socio-economic impacts of floods in a timely manner (Kussul et al., 2011). This study demonstrates how remote sensing and GIS analysis can be automated as an ArcGIS toolbox to help improve rapid response flood disaster assessment across the entire Lower Mekong River Basin (LMB).

Current Practices

During and immediately after a flood disaster, it is essential to know where and how many people the flood affected in order to maximize efficacy of relief efforts. Estimating the population and other socio-economic damage measures is a daunting task,

especially for flood disasters as expansive as those in Southeast Asia. Currently, estimates for the number of people affected by flooding in Southeast Asia are done individually by each country, and rely upon ground estimations reported by smaller administrative designations (ACAPS, 2011; MRC, 2015). Estimations of flood extent and socio-economic impacts from the ground are extremely difficult, however, and estimations often vary among agencies (ACAPS, 2011). Also, the aggregation of this information relies upon communication among various administrative levels across an entire country. The speed, accuracy, and reliability of this process for estimating socio-economic damage, therefore, may not be adequate for rapid response and efficient allocation of resources for disaster relief. While measuring floods and damage *in situ* face these limitations for disaster situations, space-borne and airborne observations can provide a timely and consistent method for monitoring large floods through time (Brooks & Adger, 2003). With GIS datasets becoming more readily available throughout the world, integrated remote sensing GIS systems can be used for disaster rapid response and socio-economic impact analysis. By automating satellite-based flood mapping techniques with GIS analysis, both flood extent maps and socio-economic impact estimates can be generated and disseminated on a near real-time basis or for historical analysis. Finally, this approach removes the time-consuming intermediate steps that involve many people, countries, and agencies, required by current methods for obtaining these initial maps and estimations.

To increase the speed of this analysis and make it easy to use, I created a tool for ArcGIS using the Python programming language. This tool requires a geodatabase that contains population distribution and other infrastructure and socio-economic data for a country, and a flood map as a shapefile for a flood event. The automation then produces

damage estimates and maps. This tool was tested for the 2011 and 2013 major flood events in Cambodia (Figure 5.1).

Figure 5.1: Study area of Cambodia, outlined in magenta.

METHODOLOGY

Deriving Flood Map

To create flood extent maps for the 2011 and 2013 events, I employed the mapping method proposed in Chapter 3. This method was used to produce flood maps at 250m resolution from MODIS 8-day composites from October 16, 2011 (Figure 5.2), and October 8, 2013. Then this map was integrated into a GIS containing socio-economic data for the region, where automated analysis produce impact estimates, maps, and

figures. By automating both the flood detection and GIS analysis, non-experts can easily obtain this information for the time period of interest nearly instantaneously.

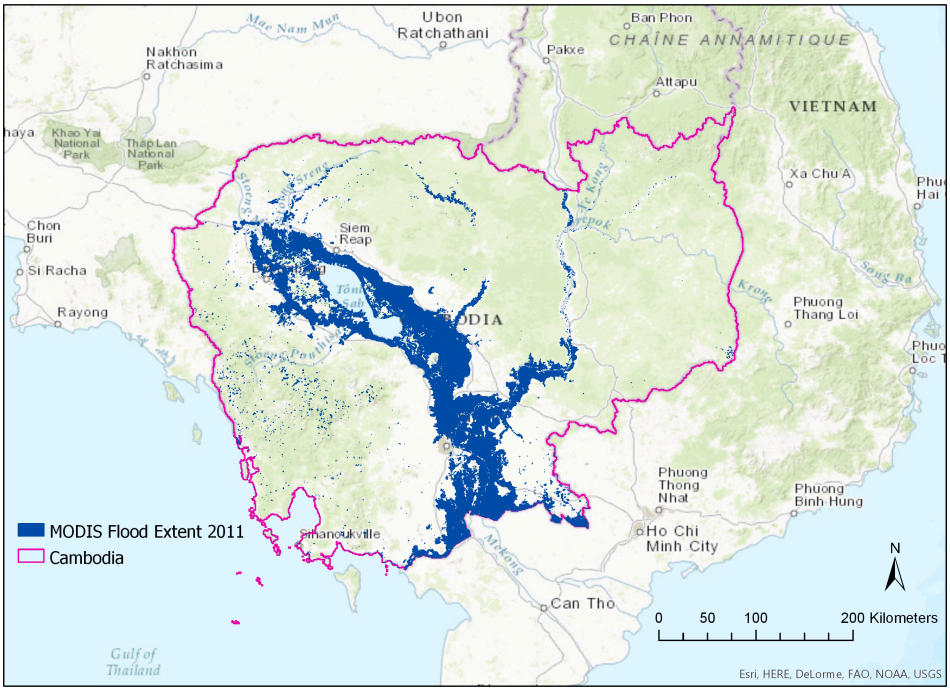

Figure 5.2: Flood extent derived from 8-day MODIS composite from October 16, 2011.

Estimating Socio-economic Impacts

I created a geodatabase to aggregate socio-economic information in a spatial format for Cambodia. Much data are available for free from various government and NGO agencies, and using open source data demonstrates how these methods can be applied to other regions. Once the data were uniformly formatted and projected, I automated GIS processes in the Python coding language to intersect a flood map with the data layers and estimate socio-economic impacts at the resolution of user-defined administrative boundary levels.

As estimating the number of people affected in different locations is essential for coordinating disaster relief, I acquired population distribution data from the WorldPop Project for Cambodia in 2010 (http://www.worldpop.org.uk). The WorldPop project uses various weighting datasets in combination with census data to create population distribution estimates by country at a 100m resolution (Figure 5.3). The estimations adjusted to match the official UN estimates were downloaded by country from the WorldPop website (http://www.worldpop.org.uk). Because this dataset and the flood extent maps are at different resolutions, several processing steps were necessary to compare the data.

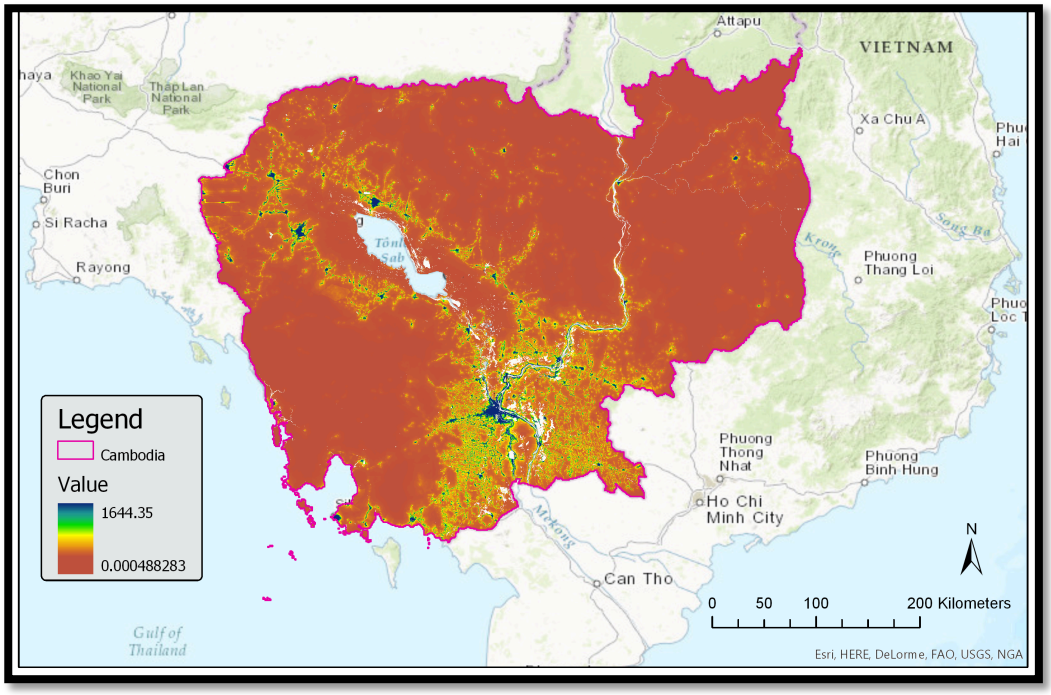

Figure 5.3: People per 100m x 100m pixel in Cambodia acquired from WorldPop (www.worldpop.org.uk)

First, I converted the population raster into a shapefile in ArcGIS, and projected to WGS 1984 UTM Zone 48N. But, adjacent pixels that have the same population value

will be joined as a single polygon feature in the shapefile, but the "GRIDCODE" value remains as the number of people in a single pixel. So, it was necessary to multiply the "GRIDCODE" by the "COUNT" to obtain the number of people in each polygon feature. Additionally, I calculated the area of each polygon in square kilometers. This shapefile was then saved in a geodatabase used as reference for the analysis.

Adding to the population data, I acquired the locations of schools and health facilities in Cambodia through the Humanitarian Data Exchange (data.humdata.org/). These datasets are provided as point shapefiles, and were projected to WGS 1984 UTM Zone 48N and added to the reference geodatabase. Cambodia province, district, and commune boundary data were also added to the reference geodatabase.

In ArcPro, I created a new Python Toolbox and opened the source code to edit with IDLE. For ease of use, the tool only requires 3 inputs: the reference geodatabase, the flood map to be used for the analysis, and the folder in which the user would like to save the results to (Figure 5.4).

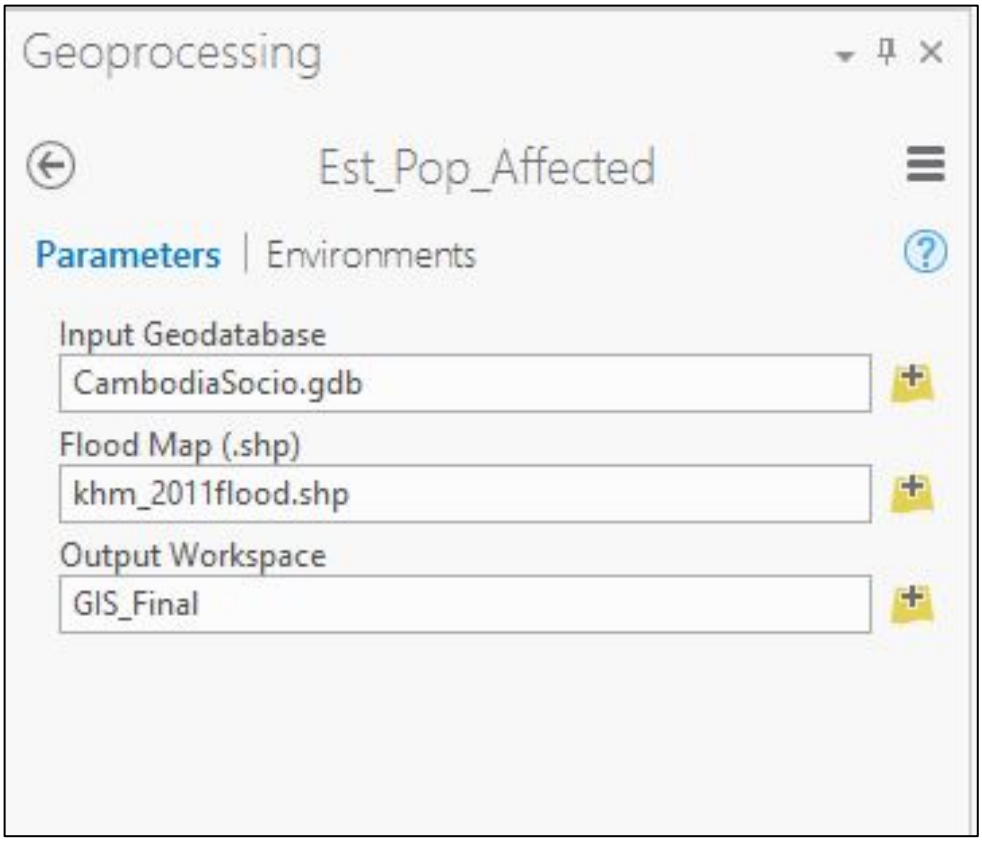

Figure 5.4: User-defined input parameters for flood impact estimation tool.

I then used the ArcPy module in Python to automate the estimation of affected people, schools, and hospitals with the user-defined flood map. First, I intersected the flood map shapefile with the population distribution shapefile. Using the area of the intersected polygons compared to the original area of the population polygons, I calculated the percent of each population polygon that is flooded. Then I multiplied this percentage by the number of people in each polygon to get the number of people affected by the flood in each polygon (Figure 5.5). The number of people affected in each polygon were summed to calculate the total number of people affected by the flood for the event in Cambodia. This method assumes an even distribution of people across each 100m x 100m pixel, but allows me to take into account the difference in resolution between the

data. Additionally, this approach allows for the input of a flood map at any resolution, not just from MODIS.

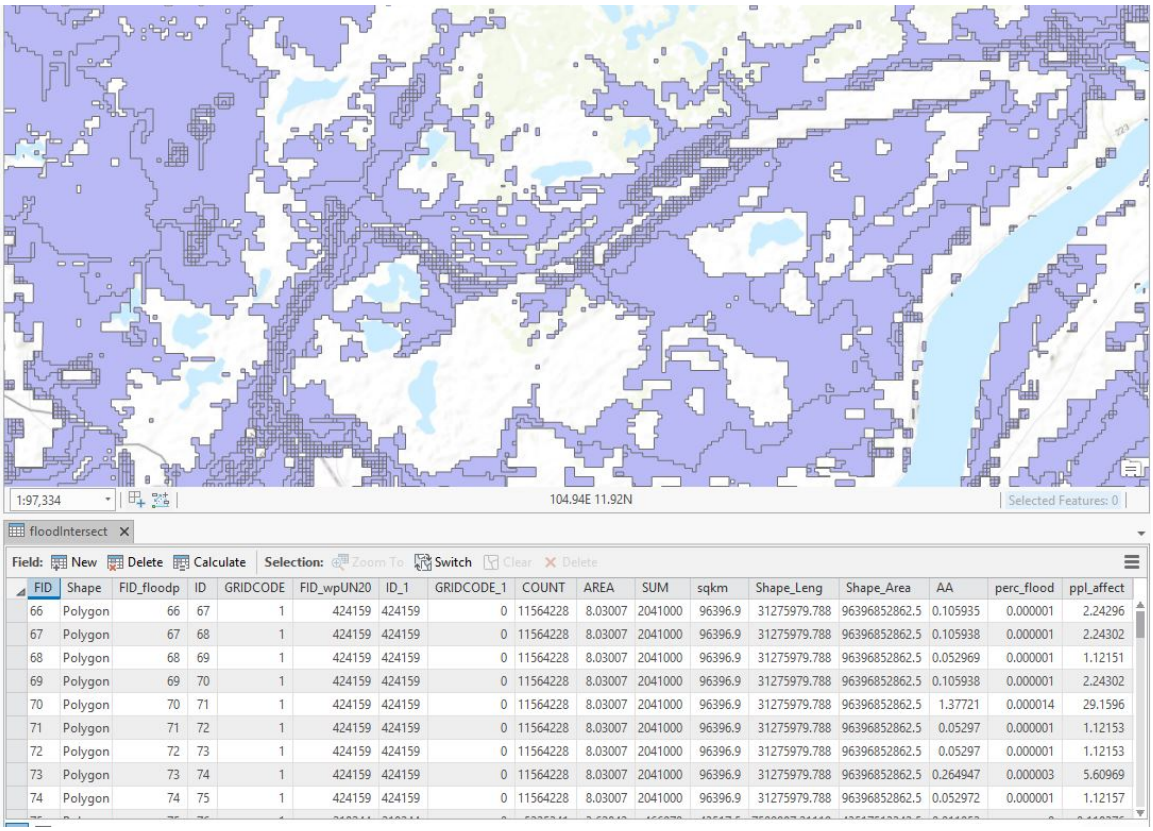

FID	Shape	FID_floodp	ID	GRIDCODE	FID_wpUN20	ID_1	GRIDCODE_1	COUNT	AREA	SUM	sqkm	Shape_Leng	Shape_Area	AA	perc_flood	ppl_affect
66	Polygon	66	67	1	424159	424159	0	11564228	8.03007	2041000	96396.9	31275979.788	96396852862.5	0.105935	0.000001	2.24296
67	Polygon	67	68	1	424159	424159	0	11564228	8.03007	2041000	96396.9	31275979.788	96396852862.5	0.105938	0.000001	2.24302
68	Polygon	68	69	1	424159	424159	0	11564228	8.03007	2041000	96396.9	31275979.788	96396852862.5	0.052969	0.000001	1.12151
69	Polygon	69	70	1	424159	424159	0	11564228	8.03007	2041000	96396.9	31275979.788	96396852862.5	0.105938	0.000001	2.24302
70	Polygon	70	71	1	424159	424159	0	11564228	8.03007	2041000	96396.9	31275979.788	96396852862.5	1.37721	0.000014	29.1596
71	Polygon	71	72	1	424159	424159	0	11564228	8.03007	2041000	96396.9	31275979.788	96396852862.5	0.05297	0.000001	1.12153
72	Polygon	72	73	1	424159	424159	0	11564228	8.03007	2041000	96396.9	31275979.788	96396852862.5	0.05297	0.000001	1.12153
73	Polygon	73	74	1	424159	424159	0	11564228	8.03007	2041000	96396.9	31275979.788	96396852862.5	0.264947	0.000003	5.60969
74	Polygon	74	75	1	424159	424159	0	11564228	8.03007	2041000	96396.9	31275979.788	96396852862.5	0.052972	0.000001	1.12157

Figure 5.5: Results of intersection between flood map and population data, and attribute table with calculations of people affected in each polygon.

To estimate the number of schools and hospitals affected by the flood, these datasets were clipped to the extent of the flood shapefile. The resulting clips contain the schools and hospitals affected by the flood, and the attribute tables contain the names of each facility, as well as the province, district, and village they are in, and additional information on each location. The tool then creates a new geodatabase titled "FloodImpactResults.gdb" in the user-defined output folder, and saves the schools and

hospitals affected to it. The results for number of affected people, percent of population, schools, and hospitals are also saved as a table in .csv format titled "CambodiaResults.csv" in the output folder.

Next, the script uses the "Extract by Mask" function to extract the population density from the original population density raster using the flood extent. This file is then saved to the results geodatabase. Lastly, "Zonal Statistics As Table" is used to determine the number of people affected in each province, and the table is joined to the province shapefile, and saved to the results geodatabase. The same process is carried out at the district and commune level. In the end, the output folder contains the results summarized in a .csv table, and a geodatabase that contains shapefiles of the affected hospitals and schools, a raster of people per pixel in flood zone, and province, district, and commune shapefiles that contain the number of people affected in each administration zone.

RESULTS AND DISCUSSION

It is difficult to validate the quantitative estimates of people, schools, and hospitals affected by the flood. To gain insight into if these estimations are at least reasonable, I compared my results to reports from the Asia Development Bank (ADB) (ADB, 2014), Red Cross (International Federation of Red Cross and Red Crescent Disaster Relief Emergency Fund, 2011), and the UN Office of Communication for Humanitarian Affairs (OCHA) for the 2011 event (OCHA, 2011)(Table 5.1), and OCHA for the 2013 event (OCHA, 2013)(Table 5.2).

Table 5.1: Impact estimates of 2011 flood in Cambodia compared to NGO reports.

Cambodia	GIS Estimates	Asia Development Bank	Red Cross	UN OCHA
Population	1,648,826	1.5-1.7 million	>1.2 million	1 million

Schools	78	1,396
Hospitals	71	115

Table 5.2: Impact estimates of 2013 flood in Cambodia compared to public reports.

Cambodia	**GIS Estimates**	**UN OCHA**
Population	1,236,936	1.7 million
Schools	607	
Hospitals	47	

The estimates for both the 2011 and 2013 events calculated by my ArcPro tool agreed well with reports from various sources (Table 5.1; Table 5.2). It is difficult to compare these results directly, however, as the methods for collecting these data are different for each organization, and the reliability of these estimates is unknown. But, the population-affected estimates are very similar and suggest that these GIS-based results are very realistic. The schools and hospitals did not agree perfectly, but this is likely because the reference datasets used in the geodatabase are incomplete. This application demonstrates the need to increase the availability of accurate spatial data to fully leverage the use of GIS in disaster relief and recovery. Regardless, these results suggest that this tool can be used to achieve realistic estimates in a timely manner through an easy to use automated process. While on the ground estimates can take a very long time to collect and the reliability is unknown, this GIS tool can provide estimations immediately across the entire country after, and evening during a disaster.

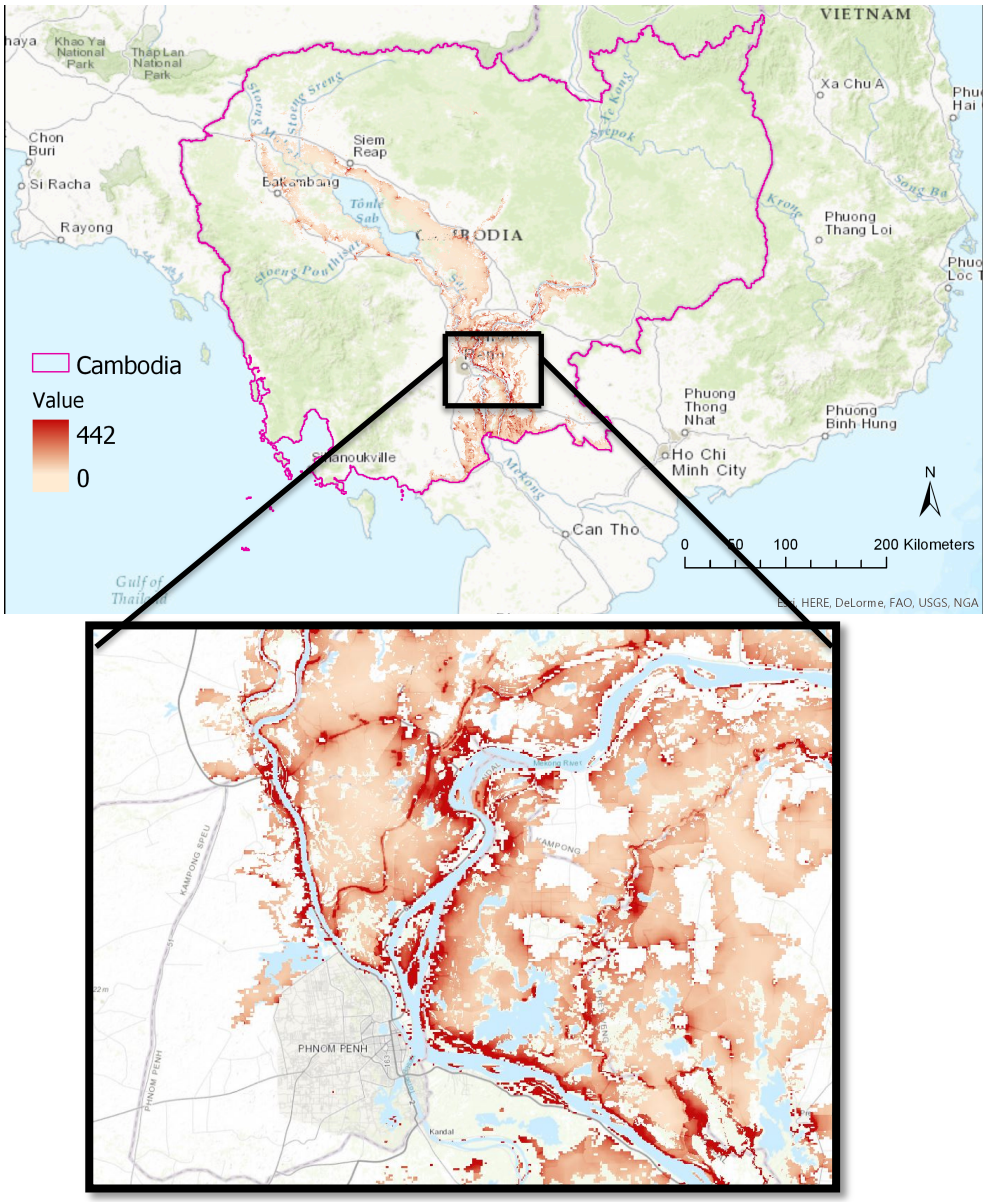

Figure 5.6: Number of people affected by 2011 flood in Cambodia in each 100m x 100m pixel.

The data provided in the results geodatabase can be used to visualize the flood impacts in different ways. The "popInFlood" raster reveals the number of people affected throughout the country at 100m resolution. This map shows how the capital of Phnom

Penh is relatively well protected, while the rural farming communities along the river are at greatest risk (Figure 5.6). In addition, the other shapefiles in the results geodatabase can be used to see the location of affected schools and hospitals, or visualize the total number affected at different administrative levels, such as provinces (Figure 5.7).

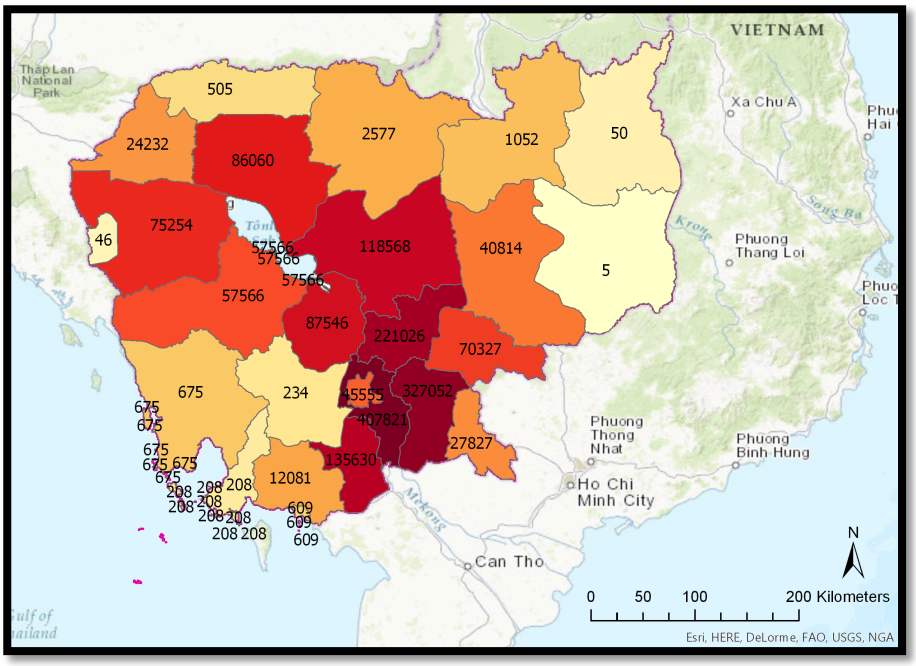

Figure 5.7: Total number of people affected by 2011 flood by province.

CONCLUSIONS

Automated geospatial analysis tools are a fast and reliable way to provide valuable information for rapid disaster assessment. This tool implemented in ArcPro can be used to calculate socio-economic impacts in Cambodia in a timely and easy to use way using flood maps at any resolution. Tools such as this can help speed up analysis time for increasing testing of methods and results, but also allows non-expert end users to perform complex analyses to obtain value results and maps.

The population affected estimates by flood disasters in Cambodia for 2011 and 2013 agreed well with public reports from various agencies, suggesting great utility for this method for disaster recovery. In addition, the agency reports were produced months after the flood events, and the during-flood estimates are not always available and generally poor. This method allows for uniform estimation of flood impacts during a flood, as well as after, in a matter of minutes with minimal manual analysis.

Future work involves expanding this tool to other countries. I will also add more data to the socio-economic database from various sources such as Open Street Map, and use higher resolution flood maps derived from radar. An advantage of the Python coding language is that the tool can also integrate into near real-time flood mapping systems to provide damage estimates in near real-time on the web. While on-the-ground coordination is essential for effective disaster response, GIS tools can drastically improve the access to, production speed, and reliability of critical information.

Chapter 6: Concluding Remarks

Floods cause more damage and humanitarian losses than any other weather-related disaster (UNISDR, 2015). Projected climate change and increased populations are expected to increase risk to floods in many parts of the world over the next century (IPCC, 2014). The Lower Mekong River Basin is one region that is particularly susceptible to flood disasters. While the people of the basin have a long and intimate connection with the seasonal flooding of the river, extreme events can be devastating. Annual flooding replenishes soils, fisheries, and reservoirs, maintaining healthy ecosystems and supporting the people and economies of the LMB (Mekong River Commission (MRC), 2011). While the ecosystem services provided by the river are greater than losses, extreme events can cause widespread casualties, displacement of people, damage to infrastructure, and loss of agriculture production (Mekong River Commission (MRC), 2012). The Mekong River flows through 6 countries, and with increased land use change and hydropower development, transboundary management of the basin is essential for both maintain the benefits of flooding, as well as responding to disasters. In an area as large as the LMB, geospatial technology such as satellite remote sensing and GIS provide powerful tools for basin-scale flood monitoring and assessment.

The results of my research demonstrate both the need for continuous monitoring of the annual flooding of the Mekong, as well as methods to help address this need. Stream gauge data does not show a significant directional trend in the magnitude or timing of the seasonal flooding, but suggest that the variability of these measures has increased over the last several decades. It is difficult to attribute a direct cause to this observation, but is likely due to a combination of land-use change, hydropower development, and climate change. As such, continuous monitoring of the river flooding is

essential for effective basin management and disaster response. I demonstrated that seasonal changes in MODIS NDVI provide an effective way to monitor the extent and relative degree of flooding across the basin from space. By doing so, we can assess historic events and flood risk as well as provide spatial flood information in near real-time. In addition, MODIS NDVI can be used to locate agricultural areas that are experiencing abnormal flooding and drought. Lastly, I provide a GIS tool to use the satellite derived flood maps to rapidly assess socio-economic damage from extreme floods. While flood risk in the LMB is expected to only increase, leveraging the utility of satellite remote sensing and GIS technologies can provide basin-scale information in a timely and reliable manner. Continuing to develop the capacity of geospatial technologies will be essential for effective basin management and humanitarian response in flood-prone regions such as the Lower Mekong River Basin.

References

ACAPS. (2011). Secondary Data Review: Cambodia, 1–20.

ADB. (2014). Cambodia: Flood damage emergency reconstruction project. *Asian Development Bank*, (March), http://www.adb.org/projects/46009-001/activities.

Arias, M. E., Cochrane, T. a., Kummu, M., Lauri, H., Holtgrieve, G. W., Koponen, J., & Piman, T. (2014). Impacts of hydropower and climate change on drivers of ecological productivity of Southeast Asia's most important wetland. *Ecological Modelling*, *272*, 252–263. http://doi.org/10.1016/j.ecolmodel.2013.10.015

Arias, M. E., Cochrane, T. a., Piman, T., Kummu, M., Caruso, B. S., & Killeen, T. J. (2012). Quantifying changes in flooding and habitats in the Tonle Sap Lake (Cambodia) caused by water infrastructure development and climate change in the Mekong Basin. *Journal of Environmental Management*, *112*, 53–66. http://doi.org/10.1016/j.jenvman.2012.07.003

Asner, G. P. (2001). Cloud cover in Landsat observations of the Brazilian Amazon. *International Journal of Remote Sensing*, *22*(18), 3855–3862. http://doi.org/10.1080/01431160010006926

Boschetti, M., Nutini, F., Manfron, G., Brivio, P. A., & Nelson, A. (2014). Comparative analysis of normalised difference spectral indices derived from MODIS for detecting surface water in flooded rice cropping systems. *PLoS ONE*, *9*(2). http://doi.org/10.1371/journal.pone.0088741

Brakenridge, R., & Anderson, E. (2006). MODIS-based flood detection, mapping and measurement: the potential for operational hydrological applications. *Transboundary Floods: Reducing Risks Through Flood Management*, 1–12. http://doi.org/10.1007/1-4020-4902-1_1

Brooks, N., & Adger, W. N. (2003). *Country level risk measures of climate-related natural disasters and implications for adaptation to climate change*. Tyndall Centre for Climate Change Research Norwich.

Brunier, G., Anthony, E. J., Goichot, M., Provansal, M., & Dussouillez, P. (2014). Recent morphological changes in the Mekong and Bassac river channels, Mekong delta: The marked impact of river-bed mining and implications for delta destabilisation. *Geomorphology*, *224*, 177–191. http://doi.org/10.1016/j.geomorph.2014.07.009

Buckley, B. M., Fletcher, R., Wang, S. S., & Zottoli, B. (2014). Monsoon extremes and society over the past millennium on mainland Southeast Asia. *Quaternary Science Reviews*, *95*, 1–19. http://doi.org/10.1016/j.quascirev.2014.04.022

Domenikiotis, C., Loukas, a, & Dalezios, N. R. (2003). The use of NOAA/AVHRR satellite data for monitoring and assessment of forest fires and floods. *Natural Hazards and Earth System Sciences*, *3*, 115–128. http://doi.org/10.5194/nhess-3-115-2003

Dugan, P., Delaporte, A., Andrew, N., O'Keefe, M., & Welcomme, R. (2010). *Blue Harvest: Inland Fisheries as an Ecosystem Service. Dep/1316/Na*. Penang, Malaysia: United Nations Environment Programme.

Dung, N. V., Merz, B., Bárdossy, a., & Apel, H. (2015). Handling uncertainty in bivariate quantile estimation – An application to flood hazard analysis in the Mekong Delta. *Journal of Hydrology*, *527*, 704–717. http://doi.org/10.1016/j.jhydrol.2015.05.033

Fayne, J. V, Bolten, J. D., Doyle, C. S., Fuhrmann, S., Rice, M. T., Houser, P. R., & Lakshmi, V. (2017). Flood mapping in the lower Mekong River Basin using daily MODIS observations. *International Journal of Remote Sensing*, *38*(6), 1737–1757. http://doi.org/10.1080/01431161.2017.1285503

Hostache, R., Matgen, P., & Wagner, W. (2012). International Journal of Applied Earth Observation and Geoinformation Change detection approaches for flood extent mapping : How to select the most adequate reference image from online archives ? *International Journal of Applied Earth Observations and Geoinformation*, *19*, 205–213. http://doi.org/10.1016/j.jag.2012.05.003

Huang, C., Chen, Y., & Wu, J. (2014). Mapping spatio-temporal flood inundation dynamics at large river basin scale using time-series flow data and MODIS imagery. *International Journal of Applied Earth Observation and Geoinformation*, *26*, 350–362. http://doi.org/10.1016/j.jag.2013.09.002

ICEM. (2013). *USAID Mekong ARCC Climate Change Impact and Adaptation Study for the Lower Mekong Basin: Main Report*. Bangkok: USAID Mekong ARCC Project. Retrieved from www.mekongarcc.net/resource

International Federation of Red Cross and Red Crescent Disaster Relief Emergency Fund. (2011). DREF operation update Cambodia : Floods 2011.

IPCC. (2014). *Climate Change 2014: Impacts, Adaptation, and Vulnerability. Part B: Regional Aspects. Contribution of Working Group II to the Fifth Assessment REport of the Intergovernmental Panel on Climate Change*. (V. R. Barros, C. B. Field, D. J. Dokken, M. D. Mastrandrea, K. J. Mach, T. E. Bilir, … L. L. White, Eds.)*Climate Change 2014: Impacts, Adaptation, and Vulnerability*. Cambridge, UK and New York, NY, USA: Cambridge University Press.

Ji, L., Zhang, L., & Wylie, B. (2009). Analysis of Dynamic Thresholds for the Normalized Difference Water Index. *Photogrammetric Engineering & Remote Sensing*, *75*(11), 1307–1317. http://doi.org/10.14358/PERS.75.11.1307

Kite, G. (2001). Modelling the mekong: Hydrological simulation for environmental impact studies. *Journal of Hydrology*, *253*, 1–13. http://doi.org/10.1016/S0022-1694(01)00396-1

Klein, I., Dietz, A., Gessner, U., Dech, S., Kuenzer, C., Klein, I., … Kuenzer, C. (2015). Results of the Global WaterPack : a novel product to assess inland water body

dynamics on a daily basis, *7058*(October). http://doi.org/10.1080/2150704X.2014.1002945

Klein, I., Dietz, A. J., Gessner, U., Galayeva, A., Myrzakhmetov, A., & Kuenzer, C. (2014). Evaluation of seasonal water body extents in Central Asia over the past 27 years derived from medium-resolution remote sensing data. *International Journal of Applied Earth Observation and Geoinformation*, *26*, 335–349. http://doi.org/10.1016/j.jag.2013.08.004

Kuenzer, C., Campbell, I., Roch, M., Leinenkugel, P., Tuan, V. Q., & Dech, S. (2013). Understanding the impact of hydropower developments in the context of upstream–downstream relations in the Mekong river basin. *Sustainability Science*, *8*(4), 565–584. http://doi.org/10.1007/s11625-012-0195-z

Kuenzer, C., Guo, H., Huth, J., Leinenkugel, P., Li, X., & Dech, S. (2013). Flood mapping and flood dynamics of the mekong delta: ENVISAT-ASAR-WSM based time series analyses. *Remote Sensing*, *5*(2), 687–715. http://doi.org/10.3390/rs5020687

Kussul, N., Shelestov, A., & Skakun, S. (2011). Flood monitoring from SAR data. In *Use of Satellite and In-Situ Data to Improve Sustainability* (pp. 19–29). Springer.

Leinenkugel, P., Wolters, M. L., Oppelt, N., & Kuenzer, C. (2015). Tree cover and forest cover dynamics in the Mekong Basin from 2001 to 2011. *Remote Sensing of Environment*, *158*, 376–392. http://doi.org/10.1016/j.rse.2014.10.021

Lu, X. X., Li, S., Kummu, M., Padawangi, R., & Wang, J. J. (2014). Observed changes in the water flow at Chiang Saen in the lower Mekong: Impacts of Chinese dams? *Quaternary International*, *336*, 145–157. http://doi.org/10.1016/j.quaint.2014.02.006

Mainuddin, M., Kirby, M., & Hoanh, C. T. (2011). Adaptation to climate change for food security in the lower Mekong Basin. *Food Security*, *3*(4), 433–450. http://doi.org/10.1007/s12571-011-0154-z

Mekong River Commission (MRC). (2010). *State of the basin report 2010*. http://doi.org/ISSN 1728:3248

Mekong River Commission (MRC). (2011). *Planning Atlas of the Lower Mekong River Basin*.

Mekong River Commission (MRC). (2012). Working Paper 2011-2015: The Impact & Management of Floods & Droughts in the Lower Mekong Basin & The Implications of Possible Climate Change. *MRC Flood Management and Mitigation Programme*.

Mekong River Commission (MRC). (2009). Adaptation to climate change in the countries of the Lower Mekong Basin. *MRC Management Information Booklet Series*, (1), 1–8.

Mekong River Commission. (2015). *Annual Mekong Flood Report 2013*.

http://www.mrcmekong.org/assets/Publications/basin-reports/Annual-Mekong-Flood-Report-2013.pdf

Naeimi, V., Leinenkugel, P., Sabel, D., Wagner, W., Apel, H., & Kuenzer, C. (2013). Evaluation of Soil Moisture Retrieval from the ERS and Metop Scatterometers in the Lower Mekong Basin. *Remote Sensing*, *5*(4), 1603–1623. http://doi.org/10.3390/rs5041603

Nguyen Thanh Long, B. D. T. (2001). Flood monitoring of Mekong river delta,Vietnam using ERS Sar data. *22nd Asian Conference on Remote Sensisng*, (November), 5–9.

Nigro, J., Slayback, D., Policelli, F., & Brakenridge, G. R. (2014). NASA/DFO MODIS near real-time (NRT) global flood mapping product evaluation of flood and permanent water detection. *Evaluation, Greenbelt, MD*.

OCHA. (2011). Cambodia 2011 Flood map, (October), 2011.

OCHA. (2013). ASIA PACIFIC REGION 15 - 21 October , 2013 Weekly Regional Humanitarian Snapshot from the OCHA Regional Office in Asia and the Pacific O C SEVEN. Retrieved from http://reliefweb.int/sites/reliefweb.int/files/resources/OCHA_ROAP_Sitmap_131021_0.pdf

Piman, T. (2014). *Climate Change Analysis in the Lower Mekong Basin: Review of Availability of Observed Meteorological Data*. Retrieved from https://books.google.com/books?id=xefUAQAACAAJ

Räsänen, T. a., & Kummu, M. (2013). Spatiotemporal influences of ENSO on precipitation and flood pulse in the Mekong River Basin. *Journal of Hydrology*, *476*, 154–168. http://doi.org/10.1016/j.jhydrol.2012.10.028

Sakamoto, T., Van Nguyen, N., Kotera, A., Ohno, H., Ishitsuka, N., & Yokozawa, M. (2007). Detecting temporal changes in the extent of annual flooding within the Cambodia and the Vietnamese Mekong Delta from MODIS time-series imagery. *Remote Sensing of Environment*, *109*(3), 295–313. http://doi.org/10.1016/j.rse.2007.01.011

Sanyal, J., & Lu, X. X. (2004). Application of Remote Sensing in Flood Management with Special Reference to Monsoon Asia: A Review. *Natural Hazards*, 283–301. http://doi.org/10.1023/B

Son, N. T., Chen, C. F., Chen, C. R., & Chang, L. Y. (2013). Satellite-based investigation of flood-affected rice cultivation areas in Chao Phraya River Delta , Thailand. *ISPRS Journal of Photogrammetry and Remote Sensing*, *86*, 77–88. http://doi.org/10.1016/j.isprsjprs.2013.09.008

Spruce, J. P., Sader, S., Ryan, R. E., Smoot, J., Kuper, P., Ross, K., … Hargrove, W. (2011). Assessment of MODIS NDVI time series data products for detecting forest defoliation by gypsy moth outbreaks. *Remote Sensing of Environment*, *115*(2), 427–

437. http://doi.org/10.1016/j.rse.2010.09.013

Sun, D., Yu, Y., & Goldberg, M. D. (2011). Deriving water fraction and flood maps from MODIS images using a decision tree approach. *IEEE Journal of Selected Topics in Applied Earth Observations and Remote Sensing*, *4*(4), 814–825. http://doi.org/10.1109/JSTARS.2011.2125778

Thompson, J. R., Green, A. J., & Kingston, D. G. (2014). Potential evapotranspiration-related uncertainty in climate change impacts on river flow: An assessment for the Mekong River basin. *Journal of Hydrology*, *510*, 259–279. http://doi.org/10.1016/j.jhydrol.2013.12.010

Thompson, J. R., Green, A. J., Kingston, D. G., & Gosling, S. N. (2013). Assessment of uncertainty in river flow projections for the Mekong River using multiple GCMs and hydrological models. *Journal of Hydrology*, *486*, 1–30. http://doi.org/10.1016/j.jhydrol.2013.01.029

Tornos, L., Huesca, M., Antonio, J., Carmen, M., Cicuendez, V., Recuero, L., & Palacios-orueta, A. (2015). Assessment of MODIS spectral indices for determining rice paddy agricultural practices and hydroperiod. *ISPRS Journal of Photogrammetry and Remote Sensing*, *101*, 110–124. http://doi.org/10.1016/j.isprsjprs.2014.12.006

Tucker, C. J. (1980). Remote Sensing of Leaf Water Content in the Near Infrared. *Remote Sensing of the Environment, 10,* 23-32.

UNISDR. (2015). The human cost of weather-related disasters 1995-2015. *UNISDR Publications*, *1*, 30. http://doi.org/10.1017/CBO9781107415324.004

Xiao, X., Boles, S., Frolking, S., Salas, W., Moore, B., Li, C., … Zhao, R. (2002). Observation of flooding and rice transplanting of paddy rice fields at the site to landscape scales in China using VEGETATION sensor data. *International Journal of Remote Sensing*, *23*(15), 3009–3022. http://doi.org/10.1080/01431160110107734

Zhang, Q., & Werner, A. D. (2015). Hysteretic relationships in inundation dynamics for a large lake–floodplain system. *Journal of Hydrology*, *527*, 160–171. http://doi.org/10.1016/j.jhydrol.2015.04.068

Zhou, M. C., Ishidaira, H., Hapuarachchi, H. P., Magome, J., Kiem, a S., & Takeuchi, K. (2006). Estimating potential evapotranspiration using Shuttleworth–Wallace model and NOAA-AVHRR NDVI data to feed a distributed hydrological model over the Mekong River basin. *Journal of Hydrology*, *327*(1–2), 151–173. http://doi.org/http://dx.doi.org/10.1016/j.jhydrol.2005.11.013

Ziv G., Baran, E., Nam, S., Rodríguez-Iturbe, I., Levin, S.A. (2012). Trading-off fish biodiversity, food security, and hydropower in the Mekong River Basin. *Proceedings of the National Academy of Sciences of the United States of America*, *109*(15), 5609-5614. doi:10.1073/pnas.1201423109.

Vita

Colin Stephen Doyle received a BS in Environmental Biology from Georgetown University in 2013. After graduation, he worked as a geospatial consultant for the NASA DEVELOP National Program at the NASA Goddard Space Flight Center (GSFC) conducting applied remote sensing research for habitat conservation and flood monitoring. He then worked for USRA Goddard Earth Science Technology and Research (GESTAR) in the Hydrological Sciences Branch at the NASA GSFC. Here, he worked on developing near real-time flood monitoring capabilities for the Lower Mekong River Basin. During his MA, Colin also worked as a Graduate Research Assistant for Dr. Timothy Beach and Dr. Sheryl Luzzadder-Beach analyzing soil and water chemistry combined with high-resolution LiDAR data to understand past and present human-environment interactions in Central America. Colin's dissertation research will focus on combining remote sensing with geochemistry and geomorphology to understand impacts of ancient Maya ecosystem engineering and water management on the modern environment.

Permanent address (or email): csdoyle@utexas.edu

This thesis was typed by Colin Stephen Doyle